Tesis Doctoral

CHARACTERIZING THE MECHANICAL RESPONSE OF EPIDERMAL CELL MONOLAYERS DURING WOUND HEALING

Autora
Leticia Valencia Blanco

Director
José Luis Jorcano Noval
Co-director
Javier Rodríguez Rodríguez

DEPARTAMENTO DE INGENIERÍA AEROESPACIAL Y BIOINGENIERÍA

Leganés (Madrid), Julio 2017

Universidad
Carlos III de Madrid
www.uc3m.es

Tesis doctoral

CHARACTERIZING THE MECHANICAL RESPONSE OF EPIDERMAL CELL MONOLAYERS DURING WOUND HEALING

Autor: Leticia Valencia Blanco

Director de Tesis: José Luis Jorcano Noval
Co-director de Tesis: Javier Rodríguez Rodríguez

Firma del Tribunal Calificador:

Firma

Presidente: Juan Carlos Lasheras

Secretario: Claudio Conti

Vocal: Gustavo Víctor Guinea

Calificación:

Leganés (Madrid), 26 de Julio de 2017

DEPARTAMENTO DE INGENIERÍA AEROESPACIAL Y
BIOINGENIERÍA
Escuela Politécnica Superior

CHARACTERIZING THE MECHANICAL RESPONSE OF EPIDERMAL CELL MONOLAYERS DURING WOUND HEALING

Autor
Leticia Valencia Blanco

Director de Tesis
José Luis Jorcano Noval
Co-director de Tesis
Javier Rodríguez Rodríguez

Leganés (Madrid), Julio 2017

To every person that has supported me during these years

"Science is not only a discipline of reason but,
also, one of romance and passion".
Stephen Hawking

"But nature is always more subtle, more intricate, more elegant
than what we are able to imagine".
Carl Sagan

Abstract

Epithelial migration plays an important role during re-epithelization phase in wound healing. Several skin diseases, such as chronic ulcers, fail during this stage. During last years a new insight into this problem has arisen introducing a mechanical point of view of this process. Kinematics and density distribution within the epithelium play key role during collective migration. Besides, the capacity of cells to proliferate and provide the tissue with new cells enhance the ability of them closing the wound.

The evolution of the leading edge have shown that experiments performed at starvation stopped at some point whereas those performed at normal condition kept advancing.

A deeper study of the velocity fields showed that, cells several rows behind the edge barely moved during the whole experiment. The experiments without proliferation showed a sudden increase in velocity that rapidly decayed after some hours while experiments at normal conditions kept a positive velocity during the whole time.

Although velocity profiles showed a completely different behaviour between experiments performed at normal conditions and at starvation, the study of density distribution of cells inside the tissue exhibit almost the same profiles. This result leads to the idea that cells acquire a well established profile to move, 'advancing formation', with lower density at the front where cells with greater velocity are found and many rows behind, confluent cells, which display slower velocity.

Cell migration results from the interplay of mechanical and chemical interactions between cells and their extracellular environment. Mathematical *in silico* models can reproduce experimental results and can predict different future behaviours. Due to the complexity and huge amount of data obtained from *in vitro* experiments, an emergent need of bioinformatics and mathematical models have appeared although experiments will always be needed. The main advantage is their ability to handle multiple interacting variables simultaneously, which is difficult to deal with in experiments. Here, we introduce the novelty of density field into Banerjee et al. model with the polarization force term proposed by Arciero et al. which mimics better our experimental results and is more physiological. The combination of both has provided good results

for the starvation case studied. The temporal evolution of the monolayer length has been fitted to obtain the set of free parameters of the model to be later used to calculate the main variables governing the problem, displacement, density and concentration of contractile units. The real size of the cell culture has shown to be an important factor to be under consideration in regulating the density distribution in the model. Besides, the study of of several parameters in the model has shown to exert little influence on the solution. Diffusivity or internal pressure could be then removed from the model without influencing significantly the results.

Transepithelial potential (TEP) is defined as the voltage across an epithelium which is the sum of all the voltages of single cell membranes. After epidermis wounding, this transepithelial potential is disrupted inducing endogeneous epithelial electric fields (EEF) that might be implicated in wound re-epithelization.

In this work we present an epithelial cell monolayer electrical characterization by means of impedance spectroscopy techniques. We have study a wide range of frequencies and three different voltages leading to the conclusion that cell monolayer exhibit a linear impedance behaviour. Given that results, we proposed an equivalent electric circuit to better understand cell-cell and cell-substrate communication. Besides, 2D wound healing assays were performed and external electric fields were applied to force different migration rates improving the ability of cells to migrate towards the wound. Finally, internal calcium concentration was monitored for the different external voltages showing higher concentration in those experiments performed with the largest electric field at the beginning of the experiments. This result suggests that cell-cell communication is enhanced by electric fields improving ion exhange and therefore improving migration rates.

This thesis has provided an important knowledge in the physics governing cell migration to Termeg group. We have started a new research line studying collective cell migration, mechanical forces or electric fields involved in the process of wound healing *in vitro*.

Resumen

La migración de células epiteliales juega un papel muy importante durante la fase de reepitelización en el proceso de cicatrización de heridas, embriogénesis, invasión de cáncer o la respuesta inmune. Muchas afecciones de la piel tales como las úlceras crónicas fallan durante esta fase. Durante los últimos años se ha dado un nuevo entendimiento a este problema estudiándolo desde un punto de vista físico y mecánico. La densidad celular y la velocidad adquirida por las células dentro del epitelio son variables esenciales durante la migración colectiva. Además, la capacidad de las células de proliferar y aportar al tejido nuevas células aumenta la habilidad de cerrar la herida. La evolución temporal de borde de la herida ha demostrado que los experimentos llevados a cabo sin proliferación se paran al cabo de cierto tiempo mientras que los que se realizaron en condiciones normales continuaron avanzando a velocidad constante.

Un estudio más detallado de los campos de velocidad mostró que, las capas de células detrás del borde de avance apenas se movieron durante todo el experimento. Los experimentos sin proliferación mostraron que inicialmente el tejido adquiere una velocidad comparable a los experimentos con proliferación pero a las pocas horas la velocidad decayó abruptamente. En cambio en los experimentos en condiciones normales las células mantuvieron una velocidad casi constante aunque también menor con el tiempo y atenuada con la distancia al borde.

A pesar de que lo perfiles de velocidad mostraron un comportamiento totalmente distinto entre los dos tipos de experimentos llevados a cabo, con y sin proliferación, el estudio de la distribución de densidades dentro del tejido mostraron perfiles muy similares. Este resultado sugiere la idea de que las células adquieren una "formación de avance" o distribución espacial de densidades bien establecida para poder migrar de manera eficiente. Este perfil muestra bajas densidades en el borde, donde se desarrollan las velocidades más altas y densidad de confluencia a una cierta distancia del mismo, donde las células apenas se mueven.

La migración celular resulta de la interacción mecanica y química entre células y el ambiente extracelular que las rodea. Los modelos matemáticos *in silico* pueden reproducir resultados observados experimentales y pueden predecir comportamientos futuros. Debido a la complejidad y la enorme cantidad de

datos que se obtienen de los experimentos *in vitro* actualmente se requieren de herramientas bioinformáticas y modelos matemáticos para sus análisis, aunque los experimentos siempre sean necesarios. La mayor ventaja es la habilidad de manejar múltiples variables que interaccionan entre sí mientras que experimentalmente es más complejo de estudiar.

En esta tesis introducimos una mejora al modelo desarrollado por Banerjee et al., incorporando una nueva variable que hemos visto que es imprescindible en la migración celular colectiva, la densidad. Además, se sustituye el término de fuerza de polarización que establece el movimiento por un término más fisiologico, propuesto por Arciero et al. y que representa mejor los fenø'menos observados en los experimentos. La combinación de ambos modelos ha proporcionado buenos resultados en la simulación de experimentos sin proliferación. Se ha realizado un ajuste a evolución temporal del borde o tamaño del tejido para obtener los valores de las constantes o parámetros libres del problema para después obtener el resto de las variables que componen el modelo, los desplazamientos, la densidad y la concentración de elementos contráctiles. Por otro lado, se ha observado que tanto la condición inicial del perfil de densidad como el tamaño real del tejido afectan de manera notoria a los resultados que el modelo es capaz de proporcionar. Finalmente se ha estudiado la influencia de los parámetros y por tanto, cierto términos de las ecuaciones del modelo, resultado que tanto la difusividad y presión interna no juegan un papel muy relevante.

El potencial transepitelial (TEP) se define como la tensión que existe a través de un epitelio que resulta ser la suma de todos los voltajes de membrana de las células que lo forman. Tras hacerse una herida en la epidermis este potencial transepitelial se perturba induciendo un campo eléctrico endógeno en el tejido que está implicado en el proceso de reepitelización de la herida.

En este trabajo presentamos la caracterización eléctrica de una monocapa celular a través de técnicas de espectroscopía de impedancia. Hemos estudiado un rango de frecuencias muy amplio y se han aplicado tres tensiones alternas diferentes donde el tejido a mostrado una impedancia lineal. A la luz de los resultados obtenidos se ha propuesto un circuito eléctrico equivalente que intenta reproducir la comunicación célula-célula y célula-sustrato. Además se han realizado experimentos de migración en los que se han aplicado campos eléctricos para forzar distintas respuestas celulares mejorando la habilidad de las células para migrar hacia el espacio libre. Finalmente, se ha monitorizado la concentración de calcio intracelular para distintos voltajes aplicados observando que

la concentración de calcio era mayor y en más células en aquellos casos donde el campos eléctrico era más elevado. Esto sólo se observó al comienzo de los experimentos , mientras que a las 24 horas la concentración de calcio era muy similar en todos los casos. Esto sugiere que el campo eléctrico dispara o acelera la comunicación célula-célula y por tanto la coordinación en la migracón.

Esta tesis ha proporcionado un conocimiento muy importante de la física subyacente en el proceso de migración para el grupo Termeg. Hemos comenzado una nueva línea de investigación en migración celular, fuerzas mecánicas o campos eléctricos involucrados en el proceso de cicatrización celular *in vitro*.

Contents

List of Figures

List of Tables

CHAPTER

ONE

General introduction

Contents

1.1 Motivation

Until 21th century the fields of cell biology and biochemistry played the major role describing the current understanding of tissue organization processes such as embryogenesis, morphogenesis, and tissue repair [20]. Mainly their explorations focused on characterizing the structure and chemistry of biological processes. Evaluating complex *in vivo* activities, especially those involving multiple interacting elements, were isolated as unworthy studies.

But, from the simplest unicellular organism to the most complex animal, all living systems interact with their physical environment so it is becoming increasingly clear that the mechanical interactions have meaningful effects on dermal tissues and may have broad pathogenic impact [26].

During the last years physicists and engineers have provided with new methods a new insight into important questions that remained open. Accurate understanding of many physiological processes must be thought as a controlled system such as the complex machinery driving wound healing.

Several factors can lead to impaired wound healing and depending on their nature, local or systemic, they can influence the characteristics of the wound or the disease state that affect the ability to heal [7]. Some skin diseases are caused by the disordered movement of cells, for example chronic ulcers, causing prolonged pressure on the tissues.

1.2 Background

1.2.1 The skin

The skin is the largest organ of the body, typically making up 15% to 20% of total body weight, with an external surface area of 1.8m^2 in adults. It has several functions but the most important is protective, being the physical barrier against the environment, controlling the passage of molecules and ions while providing protection against micro-organisms, ultraviolet radiation and toxic or mechanical agents. It is also composed by many sensory receptors that continuously examine the environment. The skin also acquires a thermoregulatory role, keeping body temperature constant. As metabolic function, for instance skin cells synthesize vitamin D, needed in many processes [1]. Skin is a dynamic organ in a constant state of change, as cells of the outer layers are continuously lost and replaced by inner cells moving up to the surface [10].

Human skin is composed of three structural layers: the epidermis, the dermis and hypodermis (figure 1.1). The epidermis is the outermost stratified squamous keratinized layer of the skin composed of cells called keratinocytes [1]. It is an important barrier between the organism and its environment, protecting it from physical, chemical, and microbial damage, and it also regulates the function and integrity of the underlying connective tissue [12]. The dermis is the layer of connective tissue that supports the epidermis and binds it to the hypodermis with and irregular surface. Finally the hypodermis consists of loose connective tissue that joins skin to subjacent organs and it is mainly composed of adipocytes [1].

1.2.2 Wound healing

Tissue restoration is one of the most complex biological processes that take place during human life. After the injury many intracellular and intercellular pathways must be activated and coordinated since skin integrity and homeostasis need to be repaired [6]. Many cell types are involved during this process,

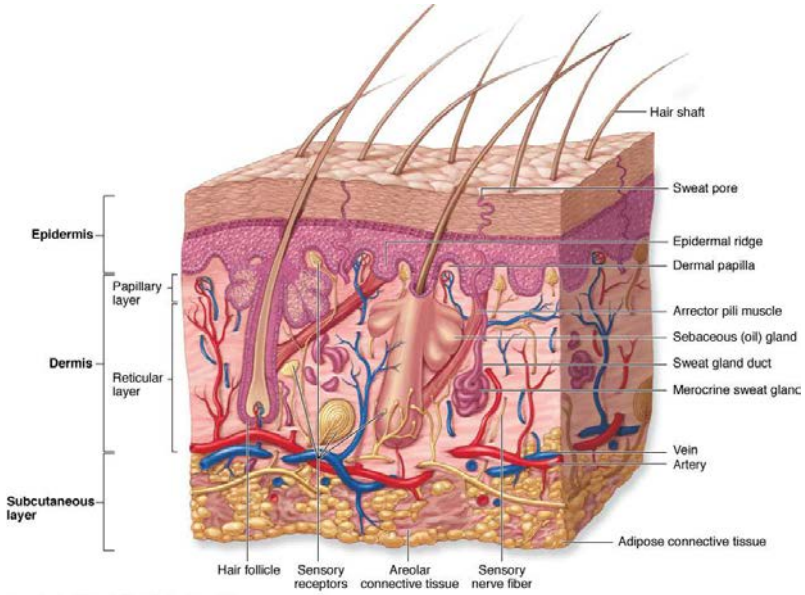

Figure 1.1: Skin layers. The outermost stratum is the epidermis, an stratified layer of keratinocytes. Underneath it is found the dermis that consists of dense irregular connective tissue and cushions the body from stress and strain. Finally the hypodermis is the innermost layer of the skin, mainly used for fat storage [1].

such as neutrophils, monocytes, lymphocytes, endothelial cells, keratinocytes and fibroblasts proliferating, differentiating and migrating, depending on their functions. Due to the complex process of wound healing, it is worth highlighting that rarely becomes uncontrolled leading to malignant formation. Injury repair provides a functional tissue with cells and a disorganized matrix, the scar.

For a wound to heal successfully, all stages must occur in the proper sequence and time frame [7]. There are three classic overlapped stages of wound repair: inflammation, granulation and remodelling (figure 1.2).

Inflammatory phase

Takes place right after wounding since vessels disruption provokes leakage of blood that coagulates due to platelet aggregation forming the fibrin clot. This clot promotes the release of cytokines and growth factors promoting immune response where cells such as leukocytes, macrophages, etc. migrate to the wound area to avoid bacteria contamination or infection (figure 1.2(a)) [20], [7].

Granulation tissue

This stage consists mainly on epithelial proliferation and migration of keratinocytes from the wound edge towards the free space over the provisional matrix (re-epithelization) (figure 1.2(b)) [20],[7].

Remodelling

The final phase is the matrix formation and restoration of the mechanical properties of an uninjured skin to approach to normal tissue architecture (figure 1.2(c)) [20],[7].

Re-epithelialization (figure 1.2(b)) after trauma or wounding has to be a robust process to restore the skin barrier function. Just right after wounding, epithelial keratinocytes are exposed to pro-migratory molecules, growth factors, cytokines and endogeneous electric fields that activate their migration towards the wound [12]. The most accepted model of re-epithelization proposes that basal keratinocytes found close to the wound edge migrate towards the wound matrix during the first 24 hours creating an epithelial tongue. Once the re-epithelization is well established basal keratinocytes found far from the edge start proliferating within the 48-72 hours after the injury to guarantee a suitable amount of cells to close the wound [12], [9].

Wound healing implicates the expression of several extracellular matrix molecules, their receptors at the membrane (integrins) and the release of growth factors. Besides, the disruption of cell-cell contacts due to the injury decreases the extracellular Ca2+ concentration, the transepithelial potential (TEP) is disrupted creating electric fields that promotes the re-epithelization process[12].

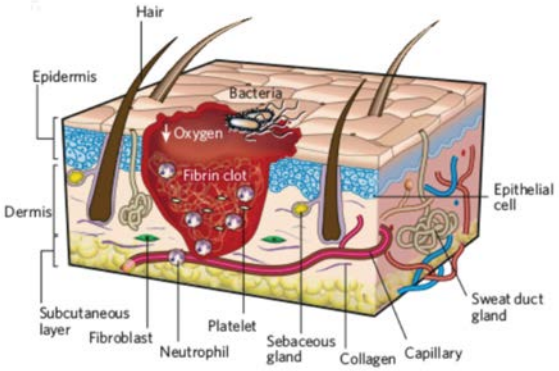

(a) Inflammatory phase

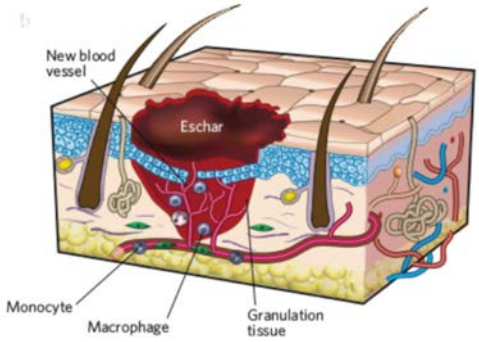

(b) Granulation tissue formation

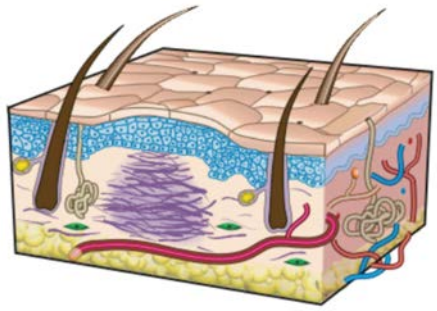

(c) Remodelling phase

Figure 1.2: There are three classic wound healing stages: inflammation (figure 1.2(a)), granulation(figure 1.2(b)) and remodelling (figure 1.2(c)) phases [6].

1.2.3 Cell migration

As mention before, cell migration plays a key role in the formation and homeostasis of multicellular organisms. Cell migration can be divided into two categories:single cell migration where cells migrate individually, and collective cell migration, in which cells move keeping tissue integrity.

Single cell migration

Single cell migration is the process by which isolated cells move through or along tissues in the body to a specific position. Although the stages of single-cell migration over a substrate has been widely studied and characterized [24], modern imaging and molecular techniques have enabled the correct visualization of this process. Formation of lamellipodium polarizes the cell that migrate into an specific direction but only long distances in the presence of chemical gradients or physical cues. For example, leukocytes are highly attracted to inflammatory chemokines released by various cells.

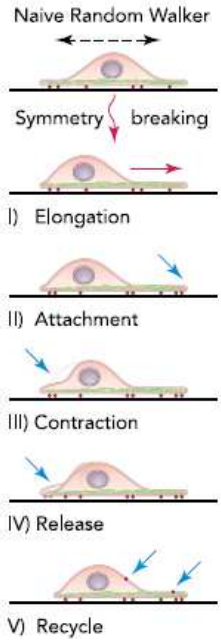

Figure 1.3: Illustration of single cell migration mechanism. Symmetry breaking lead to cell polarization and guided motion. [24].

Single-cell motion (figure 1.3) involves different steps or mechanisms:

Polarization Cells polarize towards a certain direction as a response to a spatial asymmetry in chemical concentrations, forces, electrical cues, etc. creating a clear distinction between cell front and rear. An important consequence is the extension of the membrane at the leading edge with a high concentration of polimerized actin in that region.

Protrusion Protrusion refers to membrane extensions in the direction of migration. It involves the expansion of the plasma membrane, stablishments of contact adhesions to eh substratum providing traction for the movement and actin polymerization.

Adhesion Adhesion to the substratum takes place mainly by integrin receptors in the protrusion area. It also links the substratum to the actin cytoskeleton. Around 150 different molecules are involved in cell adhesions organized into signaling complexes and regulating several pathways and processes such as microtubule dynamics or actomyosin contraction.

Contraction Cell body translocation by cell rear contraction of the actomyosin cytoskeleton is not well understood. Rear retraction requires the coordinated contraction of the actin cytoskeleton and disassembly of the adhesions at the trailing edge.

Release For productive advance of the cell body, contractoin must be coupled to release of the adhesions at the cell rear. Rear retraction requires the coordinated contraction of the actin cytoskeleton and disassembly of the adhesions at the trailing edge.

Collective cell migration

There are many biological processes involving cell displacements, such as tissue development, healing or invasion processes where cells move in groups rather than as singular cells like blood cells [21]. This movements is referred as collective cell migration since cells move together and has to coordinate their direction of motion with respect to surrounding tissues, travelling reliably large distances [21], [11],[22].

Wound healing process requires an effective cell migration towards the wound bed over long distances. Breaking the "symmetry" requires either external chemical gradients (chemotaxis), cellular confinement (haptotaxis) to direct the movement or guide cell movement in a particular direction [24]. Collective migration is crucial to maintain tissue integrity during remodelling allowing motile cells to pull immobile cells and assure adequate cell density or distribution within the tissue. This collective behaviour (figure 1.4) is an emergent

phenomenon refers to movement patterns over length scaler that are typically larger than individual cell sizes [24],[11].

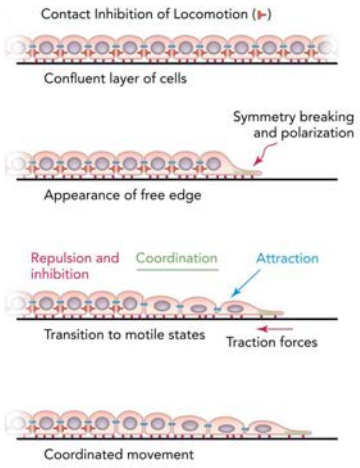

Figure 1.4: Collective migration. Cells in a confluent monolayer are subject to contact inhibition of locomotion (CIL) resulting in little migration. Availability of free space to migrate breaks the symmetry and polarizes the cells at the edge toward the free spac and promotes cell motility [24].

According to several studies, one of the most important parameters governing an ordered collective migration is the density of cells (or particles) constituting the system [24], [11]]. Although there is a local spatial coupling, characteristic in theses systems, these emerging collective movements impose a large-scale cell coordination providing strong multicellular mechanical coupling and biochemical signalling that assure a robust migration in complex environments. One of the most difficult factors studying these systems is uncoupling the mechanical contributions from the biochemical processes [11].

In vitro wound-healing assays have revealed that cell interactions with the extracellular matrix (ECM) at the cells found at the wound edge leading to cell polarization and cytoskeletal rearrangements which are typical characteristics of leader cells (figure 1.5) [16].

Defective cell migration can be a limiting event in wound healing. Therefore, *in vitro* assays studying wound healing have been widely used. A confluent cell layer is wounded under determined conditions and the migration of cells into the formerly cell-populated area is analysed [24], [2]. The cell culture surface is frequently coated with extracellular matrix components to simulate

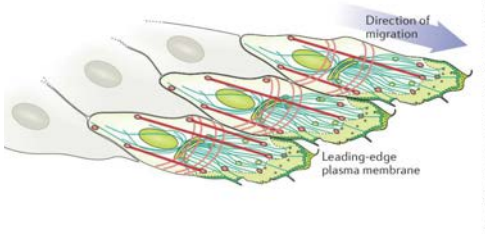

Figure 1.5: Leader cells polarization towards the wound edge direction of migration. This phenomena has been observed either *in vivo* and *in vitro* experiments [16].

and study different cell-matrix interactions. By studying the wound healing process, possible medical treatments can be screened *in vitro* before starting*in vivo* experiments. Therefore, in vitro assays are an excellent tool to study the impact of specific compounds, as well as the influence of genetic alternations on the healing process.

1.3 Scope of the thesis

The healing of acute wounds progresses smoothly, transitioning from one phase to another and resulting in stable wound closure. However, sometimes (often due to systemic conditions such as diabetes or venous insufficiency) re-epithelilization fails to complete, leading to the development of chronic, non-healing ulcers (mostly in the skin) that compromise the quality of life of the affected individuals and expose them to potentially life-threatening infections. Contrary to acute, normally healing wounds, wound edge keratinocytes in chronic ulcers are highly proliferative, are unable to migrate, and do not display markers for epidermal differentiation [12]. For this reason is so important to understand first the mechanisms governing normal wounds so that we could then study in a proper way which is the failure in chronic ulcers or cells from patients.

Practically, many aspects of the migratory behaviour of cells can conveniently be studied in vitro by using the classical "wound-healing" scratch assay, in which a confluent epithelium is scratched with a tool such as a pipette cone or a razor blade, so as to mechanically remove a "strip of cells" from the monolayer. The progression of the remaining cells during the "healing" of this "wound" is then observed under the microscope for durations ranging from a couple of hours to a few days, and the analysis of the cells' progression provides

important indications of the motile phenotype of the cells [15].

Recently, in the literature new mathematical models ([13], [5], [8], [3], [4], [22], [25], [23]) have shown up trying to reproduce and replicate cell monolayers migration applying different conditions and assumptions. These models might help understanding and predicting different behaviours such as mutations or cell-matrix interactions. We seek for a model that help us undertanding different factors affecting coordinated migration during wound healing and for latter study of skin disseases and mutations.

Additionally, when an epithelium confluency is disrupted an electrical electric field appears. Different epithelium have been characterized, showing electric fields on the order of 40 mV/mm in corneal wounds to the order of 200 mV/mm in mammalian epidermis. There is a need to better characterize the transepithelial potential(TEP) and the electrical response of cell monolayers to external electric fields in confluency and during wound healing ([14], [17], [19], [27], [18]). Endogeneous electric fields have been proposed as a new cue guiding cell migration.

In this thesis we have characterized the impedance behaviour of a cell epithelial monolayer in confluency and then we have excited with electric fields a distrupted monolayer forcing different migration rates.

1.4 Outline of the thesis

In the chapters that follow, we discuss physical aspects involved in the process of re-epithelization during *in vitro* 2D wound healing. In chapter 2, we investigate the role of proliferation in cell monolayer migration and its effects on velocity fields and cell density distribution within the epithelium. In this chapter we also explain the algorithm used to calculate the velocity field through Particle Image Velocimetry, that performs a cross-correlation between consecutive images, the maximum peak of the cross-correlation matrix provide the most likely displacement between them. Results show that although inhibition of the proliferation force the cease at some point of the cell migration, we found that the final density profile between the two different conditions are very similar.

In chapter 3, we propose a continuum mathematical model that might reproduce the results observed in the experiments shown in chapter 2. This model is mainly based on previous published model [4] with some modifications based on our experience and another model [3]. Besides the experimental results that we have observed and shown in chapter 2 were used to fit to perform the fit of free

parameters for the cases without proliferation. We obtained a system of three partial differential equations for the displacements, density and concentration of contractile elements. The results from the mathematical models reproduced very well what we observed in the laboratory and helped us quantifying some physical parameters we were not able to measure.

In chapter 4, we further explore the effect of external electric fields applied to migrating monolayer and the impedance characterization of the intact epithelium. We propose an equivalent model that allowed us to capture the phenomena driving this process. This model can be used for future analysis of illnesses, full developed 3D epithelium characterization, calcium channels influence on cell-cell communication, etc. We found that cell monolayer exhibits a linear impedance, meaning that it is independent of the applied external voltage. Then we study the influence of the external electric fields to the migration.

Lastly in chapter 5, we present a summary of the aims and contents of the dissertation providing the general conclusions and final remarks of this study. To conclude we propose future works to continue this investigation for further comprehension of the remain open questions.

Nomenclature

ECM	Extracellular Matrix
TEP	Transepithelial Potential
CIL	Contact Inhibition of Locomotion

Bibliography

[**1**] *Junqueira's basic histology: Text and atlas (Thirteenth edition.)*. âĂć, 2013.

[**2**] S. S. P. V. T. S. Anne Stamm, Kerstin Reimers and I. Pepelanova. In vitro wound healing assays - state of the art. *BioNanoMaterials*, 2016.

[**3**] B. M. H. D. Arciero J.A., Mi Q. and S. D. Continuum model of collective cell migration in wound healing and colony expansion. *Biophysical Journal*, 100:535:543, 2011.

[**4**] S. Banerjee, K. J. C. Utuje, and M. C. Marchetti. Propagating stress waves during epithelial expansion. *Phys. Rev. Lett.*, 114:228101, Jun 2015. doi: 10.1103/PhysRevLett.114.228101. URL https://link.aps.org/doi/10.1103/PhysRevLett.114.228101.

[**5**] L. K. Cai, A.Q. and H. B.D. Multi-scale modeling of awound-healing cell migration assay. *Journal of Theoretical Biology*, 245:576:594, 2007.

[**6**] Y. B. Geoffrey C. Gurtner, Sabine Werner and M. T. Longaker. Wound repair and regeneration. *Nature*, 2008.

[**7**] S. Guo and L. A. DiPietro. Factors affecting wound healing. *Journal of Dental Research*, 89:219–229, 2010.

[**8**] M. G. Habbal A., Barelli H. Assessing the ability of the 2d fisher-kpp equation to model cell-sheet wound closure. *Mathematical Biosciences*, 252:45:49, 2014.

[**9**] N. C. Y. H. R. A. G. N. A. S. S. B. P. L. K. R. R. I. Irena Pastar, Olivera Stojadinovic and M. Tomic-Canic. Epithelilization in wound healing: A comprehensive review. *Advances in Wound Care*, 2014.

[**10**] B. J. and B. P. Skin structure and function. *Aromadermatology*, 2006.

[**11**] A. J. Kabla. Collective cell migration: leadership, invasion and segregation. *R. Soc. Interface*, 2012.

[**12**] L. H. Leeni Koivisto and H. Larjava. Re-epithelialization of wounds. *Endodontic Topics*, 2012.

[**13**] B. M. and J. McGrath. Sheet migration by wounded monolayers as an emergent property of a single-cell dynamics. *J. Cell Sci*, 120:876:884, 2007.

[**14**] Z. M. Electrical fields in wound healing-an overriding signal that directs cell migration. *Seminars in Cell and Developmental Biology*, 2009.

[**15**] A. H. J. J. P. C. B. L. A. M. Poujade, E. Grasland-Mongrain and P.Silberzan. Collective migration of an epithelial monolayer in response to a model wound. *PNAS*, 104:15988–15993, 2007.

[**16**] R. Mayor and S. Etienne-Manneville. The front and rear of collective cell migration. *Nature Reviews, Molecular Cell Biology*, 2016.

[**17**] R.-A. M. S. B. . Z. M. McCaig, C. D. Controlling cell behavior electrically:current views and future potential. *Physiology Review*, 2005.

[**18**] I.-R. R. . N. R. Nishimura, K. Y. Human keratinocytes migrate to thenegative pole in direct current electric fields comparable to those measured in mammalian wounds. *Journal of Cell Science*, 1996.

[**19**] R. Nuccitelli. Endogenous ionic currents and dc electric fields in multicellular animaltissues. *Bioelectromagnetics*, 1992.

[**20**] M. D. Richard A. F. Clark. Cutaneous tissue repair. basic biologic considerations. *Journal of the American Academy of Dermatology*, 1985.

[**21**] P. Roth. Collective cell migration. *Annual Review of Cell and Developmental Biology*, 25:407:429, 2009.

[**22**] C. O. G.-M. E. S. P. H. V. Sepúlveda N., Petitjean L. Collective cell motion in an epithelial sheet can be quantitatively described by a stochastic interacting particle model. *PLOS Computational Biology*, 9:3, 2013.

[**23**] G. N. S.-P. M. G.-M. E. Shirley M., Shlomovitz R. and S. P. Physical model of the dynamic instability in an expanding cell culture. *Biophysical Journal*, 98:361:370, 2010.

[**24**] L. C. Vedula E.R.K., Ravasio A. and L. B. Collective migration: a mechanistic perspective. *Physiology*, 28:370:379, 2013.

[**25**] J. E. Vermolen F.J. Computer simulations from a finite-element model for wound contraction and closure. *Journal of Tissue Viability.*, 19:43:53, 2010.

[**26**] M. T. L. G. C. G. Victor W. Wong, Satoshi Akaishi. Pushing back: Wound mechanotransduction in repair and regeneration. *Journal of Investigative Dermatology*, 131:2186–2196, 2011.

[**27**] X. L. J. Q. C. T. Yu Wang, Guixue Wang. Substrate stiffness regulates the proliferation, migration, and differentiation of epidermal cells. *Burns*, 38:414:420, 2012.

CHAPTER

TWO

Relation between density and speed in a cell monolayer during gap closure

Contents

2.1 Introduction

Cell migration plays an important role in governing various biological processes for animal development and physiology [17]. Cells migrate to develop tissues, during the immune response and wound healing [11]. While the motion of individual cells has been widely studied ([6] ,[12]), the understanding of the collective motion of a large number of cells as is observed in tissues still present important questions open [14].

Although it has been usually considered that cells that composed an epithelium are confined and fixed in position, it has been observed that morphogenesis can involve coordinated motion in order to maintain tissue integrity [11] [4].

Collective migration is a dynamic process that requires active use of many cellular structures, such as cytoskeleton, membrane..., but also involves active

interaction with the environment. These interactions are physical (mechanics) and also chemical (signaling) which are essential for coordinated cell movement ([11], [17], [21]).

Numerous studies have attempted to explain collective cell migration from different points of view. Previous published studies believe that the formation and transmission of traction forces exerted from the front to their neighbours coordinates the overall movement of the monolayer ([16], [4]). They have reported that there is a travelling wave moving inwards the tissue that propagates the movement [8] and forces. There are many works performed in the study of the effect of growth-factors such as the one carried out by [18] that led to better migration rates and allowed to identify proteins involved in migration ([12], [18]) and force transmission. Besides, electrotaxis is a young discipline focused on the study of the impact that electric fields have on cell migration and is leading to the detection of signalling pathways and better migration rates when external electric fields are applied ([9], [3]).

Surprisingly, the effects of proliferation on cell density distribution have not been closely examined in collective cell migration. To the extent of our knowledge the only works that studied the effect of the density in the migration of a monolayer was performed by Misfeldt et al. and Tremel et al. ([10] and [15]). Misfeldt et al. [10] found that there is a threshold density necessary to start the healing below which cells did not migrate. On the contrary, the group from [15] tracked the movement of cells showing that their average effective velocity was inversely proportional to cell density. The most recently published work regarding velocity and density during monolayer migration from Tlili et al. [13] concluded that cell velocity is inversely proportional to cell radius. Besides, they observe backwards propagating velocity and density waves in antiphase.

In our particular case, we are focused on understanding the mechanisms of tissue repair in epidermal cell monolayer, which is a model problem less complex than wound healing. More specifically, the purpose of this study is to introduce a quantitative approach of the biological problem of wound healing in a cell monolayer.

The objectives of this chapter are to determine whether the proliferation in a migrating monolayer affects the density distribution and the velocity profiles established during wound healing. Qualitative data of custom-made algorithm that detects cells centroids allowed us to better understand the interplay between cell expansion(cell division inhibited) and proliferation (normal conditions).

2.2 Materials and Methods

2.2.1 Cell culture and microscopy

HaCaT cell line is an spontaneously aneuploid immortalised human epidermal keratinocytes cell line very common in in-vitro experiments due to their capability to differentiate and proliferate. HaCaT cells were grown in Dulbeco's Modified Eagles Medium (DMEM 1X, Invitrogen Life Technologies) supplemented with 10 % Fetal Bovine Serum(FBS, Thermo Scientific HyClone) and 1% of Antibiotic Antimycotic(FBS, Thermo Scientific HyClone).

When 75% of confluency is reached cells are subcultured. Medium is removed from petri disk, then 7 mL of PBS (Phosphate Buffer Serum) is added to rinse the cells and finally removed with vacuum. Then 2 mL of trypsin is added and incubated for 10 minutes at 37° C/ 5% CO_2 allowing the cells to detach from the plate. Once the cells have been detached, to inhibit trypsin action 10mL of DMEM with /10% of FBS is added to the petri disk and it is pipette up and down to remove clumps and resuspend the cells. The dilution is transferred to a 15mL Falcon tube, a sample of 10µl is used for cell counting and the rest is centrifuge at 1000 rpm for 7 minutes with a balance of the same volume. The obtained supernatant (10mL of DMEM + 2mL of trypsin) is poured off to remove trypsin and deposited cells at the bottom of the tube is resuspended in fresh medium at the more convenient concentration.

To perform cell counting a sample of 10 µL is taken and transferred to Neubauer's chamber (figure 2.1) before the centrifugation stage. To provide more statistically consistent number, at least the measurement is repeated three times.

Although there is a variety of automated cell counting instruments, hemocytometers remains the most common tool for cell counting in laboratory. Neubauer's chamber is a thick glass plate with two shaped ruled areas of $3mm^2$ divided into 9 large squares of $1mm^2$ area. Each of them is subdivided into 16 smaller squares. There is a glass cover placed on top of the chamber keeping a gap of 0.1mm between the cover slip and the ruled area.

Depending on the type of the sample a suitable concentration of cells must be prepared. If cells are too diluted, the sample size will not be enough to make strong inferences and if the sample is too crowded it will be difficult to count. In order to perform a better statistical approximation, we take three different samples to reduce the error estimating the number of cells in dilution. It is very important to control the number of seeded cells since the density is one of the

Figure 2.1: Picture of Neubauer's chamber and grid used for cell counting

parameters under study.

In order to study the influence of the proliferation in cell migration, two set of experiments were considered, normal conditions (10% FBS) and starvation (1% FBS) reducing their capability to proliferate but without inducing cell death.

Initial cell density a sensible parameter setting up the experiment that is important to control and make sure that it is the same in both cases (normal conditions and starvation). Since the cells seeded at 10% FBS are allowed to proliferate and the ones at 1% cannot, several tests were performed in order to obtain the initial density at which each set had to be seeded. Different initial densities were cultured and incubated overnight like regular experiments, the day after cell number was determined by means of Neubauer chamber and custom-made cell detection program. These tests shown that to start the experiment after 24 hours after seeding at the same density, set N should have 20% less cells than set S due to the proliferation taking place overnight.

In order to create a discontinuity in the monolayer, but avoiding possible cell death at the edge due to scratching assays, we used a soft elastic stencil, consisting of a crosslinked polydimethylsiloxane (PDMS) piece (Ellsworth Adhesive Co 184 SIL ELAST KIT).

The procedure to fabricate the stencils follows several steps:

First, mix ten parts of Sylgard prepolymer and one part of curing agent. Then, to the remove the bubbles the mixture has to be degassed with vaccum. After, pour into the molds, in our case the same petri dishes used for the experiments. Cure them at 80° C for one hour. After cooling, peel carefully the crosslinked film and using a sharp scalper cut the piece with the desired shape. Before use, the stencil has to be properly cleaned and sterilized with

UV light.

Cells are cultured in previously functionalized with collagen 35 mm plastic tissue culture plates with the stencil and incubated in 5%CO2/95% air at 37° C conditions, and after 24h the stencil is carefully removed releasing a free space to move.

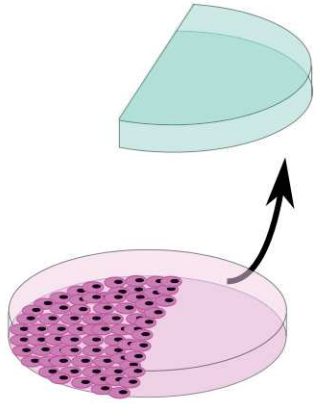

Figure 2.2: Sketch of PDMS stencil removal and semi-infinite cell culture formation

We used this controlled starvation, reducing the amount of serum in the culture media as a mean to regulate proliferation and thus force different density distributions. Considering that the eukaryote cell cycle consists of the following stages (figure 2.3) and that it last about 24 hours:

- **G1 phase**: Growth and normal metabolic activities.
- **S phase**: DNA synthesis replicates the genetic material.
- **G2 phase**: Metabolic changes enabling cell for mitosis and cytokinesis.
- **M phase**: Nuclear division (mitosis) followed by cell division (cytokinesis). It is subdivided in another four stages: prophase, metaphase, anaphase and telophase.
- **G0 phase**: or quiescent stage is the phase where cell is not dividing nor even preparing to divide.

Previous studies, such as the one accomplished in [7], demonstrate that cell cycle can be synchronized by serum starvation as well as contact inhibition or chemical treatments. Culturing cells in starvation conditions (1% of serum, set

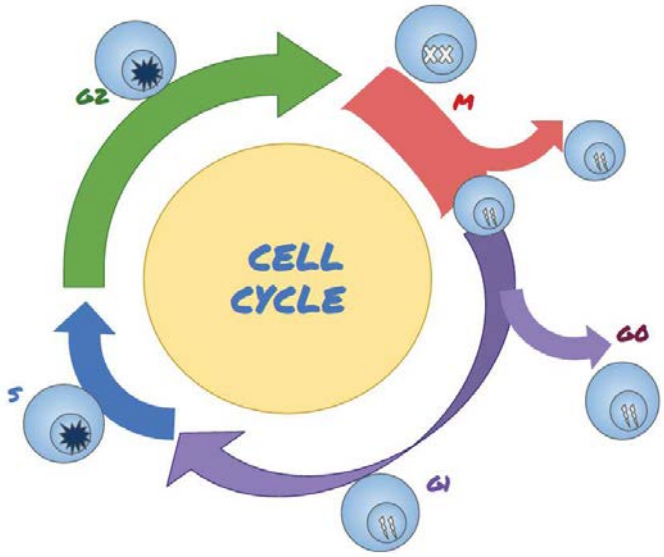

Figure 2.3: The eukariotic cell cycle phases

S) increases rapidly the proportion of cells in G0/G1 stage when compared to cycling cells (10% of serum, set N). However, the percentage of cells in G0/G1 were not increased further by prolonging the serum starvation time. There were no significant differences in the number of apoptotic cells between the two cases meaning that by decreasing the percentage of serum we are not provoking the death of the population.

In order to evaluate cell motion, after 24 hours, a discontinuity in the monolayer is carefully created by peeling the PDMS stencil and setting the cells free to move from the previous confinement. To monitor how cell tissue moves to close the free space, microscope incubator has been used to enable time-lapse. This chamber assures that the culture is at the proper conditions of humidity, temperature and air/CO_2 concentration. In particular, the equipment is a UNO Incubator from OKO Lab. This equipment is placed at an OLYMPUS CKX41 microscope within an PL-B625 electronic camera from Edmund Optics on it and an phase contrast objective. Experiments were performed for typically 72 hours.

2.2.2 BrdU immunostaining

Bromodeoxyuridine(BrdU) added to the culture media is incorporated into the DNA of cells that are in the S-phase of the cell-cycle. This procedure allows

the detection of those cells that are in division process. Cells were seeded as previously explained but on collagen functionalized coverslips with PDMS stencils adapted to them so semi-infinite wound can be performed on top it.

Two time points were studied for both set N and set S,the beginning of the experiment, t= 0 h, and the end of the experiment, t = 72 h. First, BrdU was added to the culture media at a concentration of 6µl/ml and incubated at 37°C for 2 hours. After that, cells were fixed with methanol at -–20°C for 10 minutes.

Then, fixed cultures were treated for 30 min in 1M HCl. This step separates DNA into single strands, so that the primary antibody has access to the incorporated BrdU. After that, nonspecific epitopes were blocked with with 3%BSA 0.2%Triton X-100 in PBS, for 15 min at 37°C. Primary antibody (anti-BrdU) was incubated overnight at 4°C at 6µl/ml concentration in 3%BSA-PBS. The next day, secondary antibody (anti-mouse IgG), diluted in 3%BSA-PBS at concentration of 1:50 was incubated in dark for 45 minutes at room temperature. Finally, each coverslip was counted on a microscope slide with moviol and DAPI (1:1000) (to label the nuclei). Pictures were captured on Olympus CKX-41 direct microscope equipped with Olympus U-RFL-T mercury burner with FITC and DAPI filters.

2.2.3 Image Analysis: Cell detection

Image analysis is being done using custom-made codes written in MatLab. The leading edge detection at each image was performed by using segmentation algorithms describe in [5].

From the detection of the leading edge, figure 2.4(a), the temporal evolution of its position can be obtained. This information provides the instantaneous velocity of the edge. We consider the gap to be closed when the first contact between the two edges occurs.

Most of the conclusions of this work are supported by our measurements of cell density. To quantify the number of cells in each image we use the following morphological operations [2], illustrated step by step in figure 2.4.

In order to determine cells' centroid we followed next steps treating the images:

1. First, detection of the edge of the wound to filter any noise that might be detected in there (Fig. 2.4(a)).

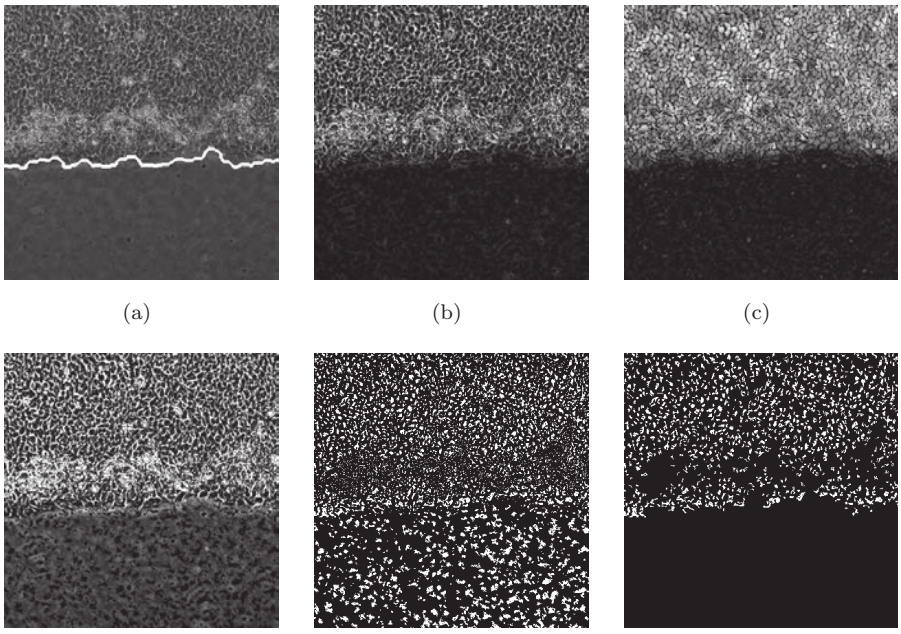

Figure 2.4: Different steps of the image processing pipeline for individual cell detection. 2.4(a) is the original image with the edge detection. 2.4(b) Contrast enhancement. 2.4(c) Gap exageration separating cells 2.4(d) Watershed transformation. 2.4(e) Threshold and filtering. 2.4(f) Binary image with individual cells isolated.

2. Second, the adjustment of the contrast to enhance objects and their borders. Obtaining as a result an image containing peaks and valleys (Fig. 2.4(b)).
3. Then, exaggeration of the gaps among cells maximizing the contrast and separating the cells (Fig. 2.4(c)).
4. Next, convert objects of interest by watershed transform in order to detect intensity valleys (Fig. 2.4(d)).
5. And after that, get rid of those objects that should not be considered (such as dead cells) by applying some thresholds and filters.
6. Finally, the measurement of properties of the objects detected from the binary image (Fig. 2.4(f)) to obtain areas, centroids, eccentricities, major and minor axes, diameters...

Once the individual detections are done, the centroids of the cells can be

plotted, figure 2.6 for visual inspection to verify that the algorithm works correctly. Despite of the change in size with time of the cells, the discontinuity present at the edge or image boundaries the detection seems to work appropriately.

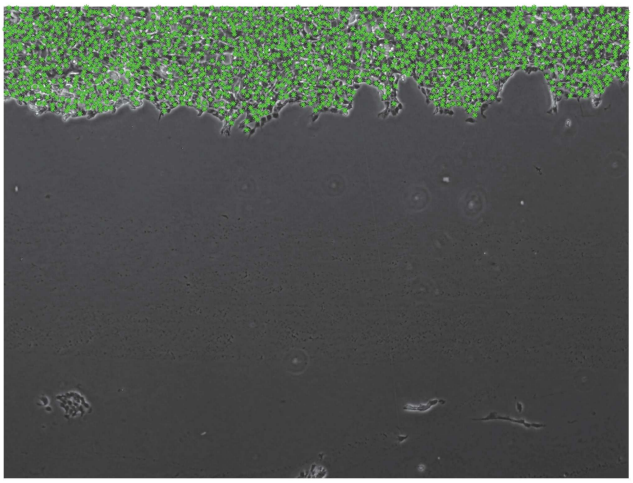

(a) Example of the results of the cell detection algorithm

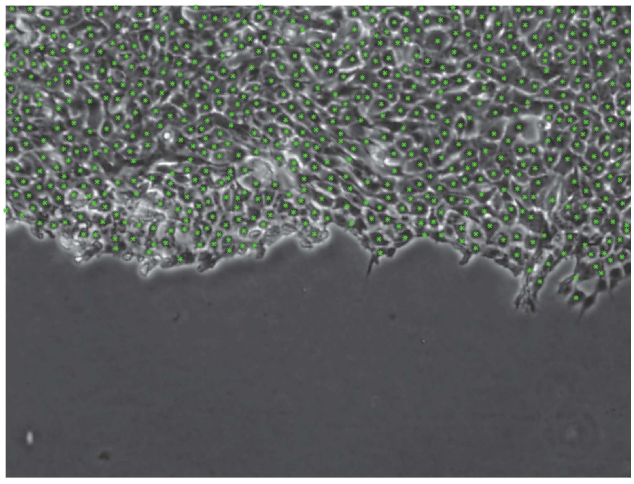

(b) Zoom of the detection near the edge

Figure 2.6: Detection of cell centroids on a sample image applying morphological operations.

To test the error in cell detection commited by the algorithm a visual counting of cells was compared to the automatic cell detection in thirty images leading to a mean error of 12.5%. If there is any death cell in the monolayer, it is filtered

and not considered in the analysis.

In figure 2.6 an example of cell detection is shown. Visually there is a good agreement between automatic detection through image segmentation techniques.

2.2.4 Particle Image Velocimetry (PIV)

Velocity fields were computed in Matlab (The MathWorks, Inc., Natick, Massachussets, United States), using the open source program PIVlab(Time-Resolved Digital Particle Image Velocimetry Tool for MATLAB), a free algorithm, developed by [19]. PIVlab is an open-source particle image velocimetry (PIV) software which calculates the velocity distribution within image pairs and calculate the cross-correlation matrix of them, thus leading to the most likely displacement in the frame.

The program gives the opportunity to load a mask in a certain region of the image where there cannot be a displacement. In our case, the mask were obtained detecting the edges of the image and the leading edge of the monolayer, the surface where there is not any cell; and then loaded into the software. In this way, the program does not compute the velocity in the masked area, avoiding possible noise or outliers in the velocity field.

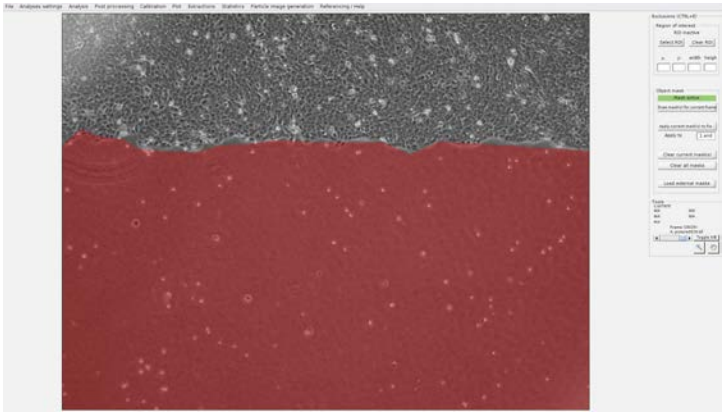

Figure 2.7: Interface showing the loading of an external mask to avoid the computation of velocity fields there.

We performed several tests varying the set-up parameters and by visual inspection and best signal-to-noise ratio we determined the most favourable combination of them for our experiments.

We fix first interrogation window to 64 pixels with a step or overlap of 32 pixels. Then only a second pass was chosen with a size of 32 pixels window, leading to a 16 pixels step between vectors. Cells size in the images are around 15-20 pixels, so this configuration yielded to barely one vector per cell.

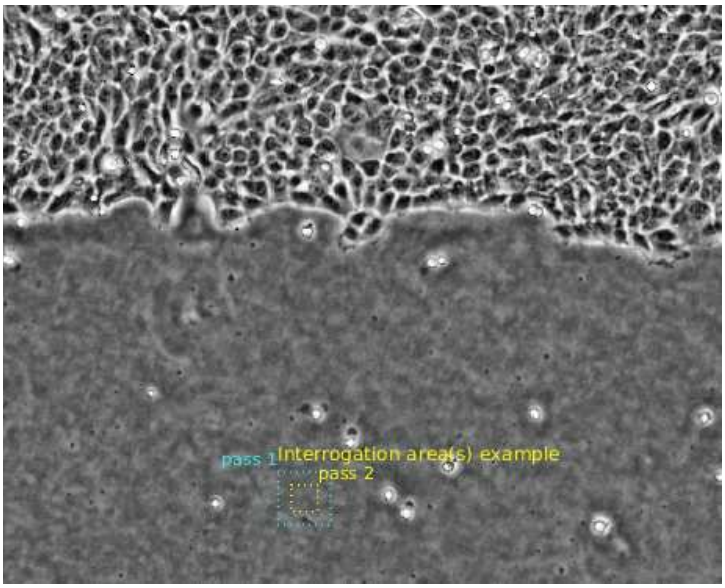

Figure 2.8: Configuration of the window sizes chosen that better fitted our experiments.

The correlation algorithm chosen for the calculations was FFT winddow deformation (direct Fourier transform correlation with multiple passes and allowing window deformation). The toolbox include a data validation section to remove those vectors that may show up due to poorly illuminated regions in the image or strong out-of-plane particles flowing. In our case we chose the standard deviation filter (setting n=7) and interpolating those of them out of limits.

2.2.5 Strip Averaged Velocity and Density Fields

Post-processing of the velocity and density datasets was carried out by custom-made programs developed in Matlab.

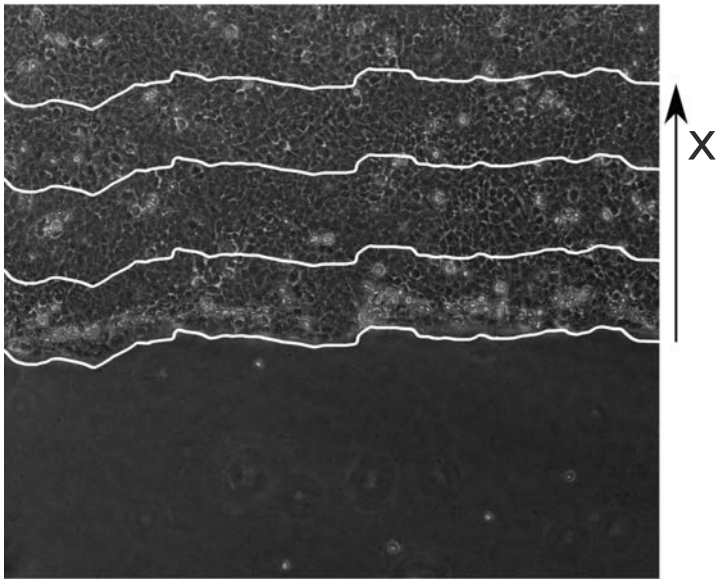

Figure 2.9: Sketch of the strips used to perform averages. The detection of the leading edge is used to create different strips throughout the interior of the monolayer. With this strips different parameters can be averaged and its dependency with the distance to the edge is measured.

In order to obtain the relation between velocity field and distance to the edge, velocities were averaged by strips. The border of the scratch is detected and, with the same shape, different strips are obtained averaging the velocity vectors or computing the number of cells inside them, figure 2.9. From now on, we will use the term depth as the concept of distance inward to the edge of the tissue ($\mathbf{x}$).

2.3 Results

We have performed a controlled starvation and normal conditions experiments as a way to regulate proliferation and thus force different cell responses. We have worked with two different sets of experiments, normal conditions (set N) at 10% of Fetal Bovine Serum(FBS) and starvation conditions (set S) at 1% FBS. Culturing cells in starvation conditions(set S) increases the proportion of cells in G0/G1 stages compared to cycling cells(set N) [7] and there are no differences in the number of apoptotic cells between the two cases.

Besides an (expected) effect in the proliferation behaviour, cells cultured in

different media exhibit interesting differences in their ability to close a gap in the monolayer.

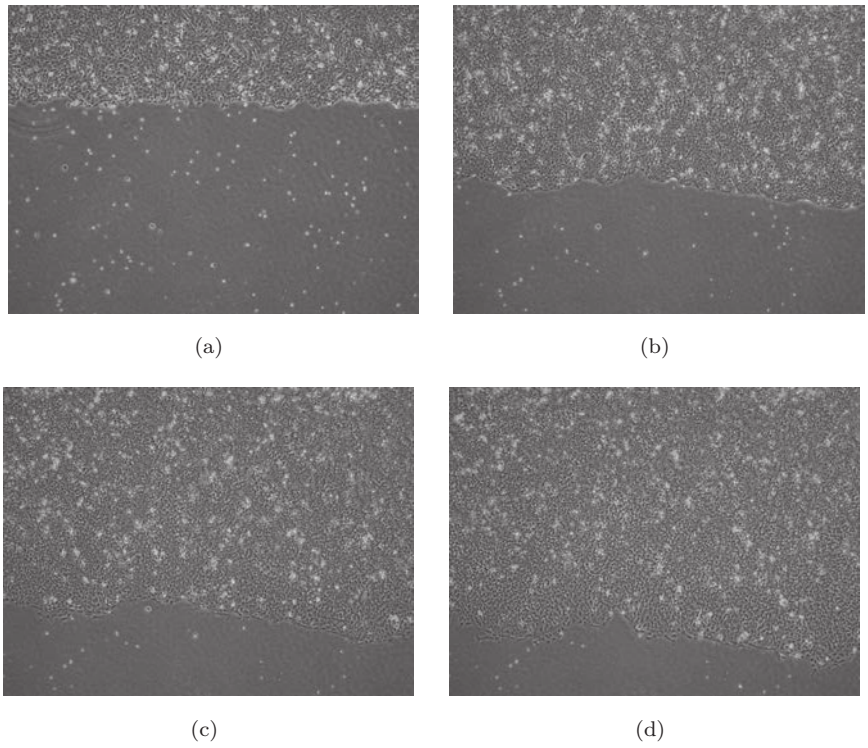

Figure 2.10: Timelapse at starvation. 2.10(a) at t= 0h, 2.10(b) at t= 16h, 2.10(c) at t= 33h and 2.10(d) at t= 50h,

In fact, whereas cells in set N always close the defect and do not stop migrating, those in set S stop their motion before that happens. This result is quantitatively illustrated in figure 2.12, where the mean position of the monolayer front is shown as a function of time for experiments belonging to the two sets.

Figure 2.12 shows clear differences in the mean edge displacement between experiments at normal conditions and those carried out in starvation. In both cases, around the 20 first hours the edge moves at relatively similar velocity from the instant when the wound is performed. In sets S, the edge starts to slow down until it is completely stopped. On the contrary, in set N the leading edge keeps advancing until the edge disappears from the field of view

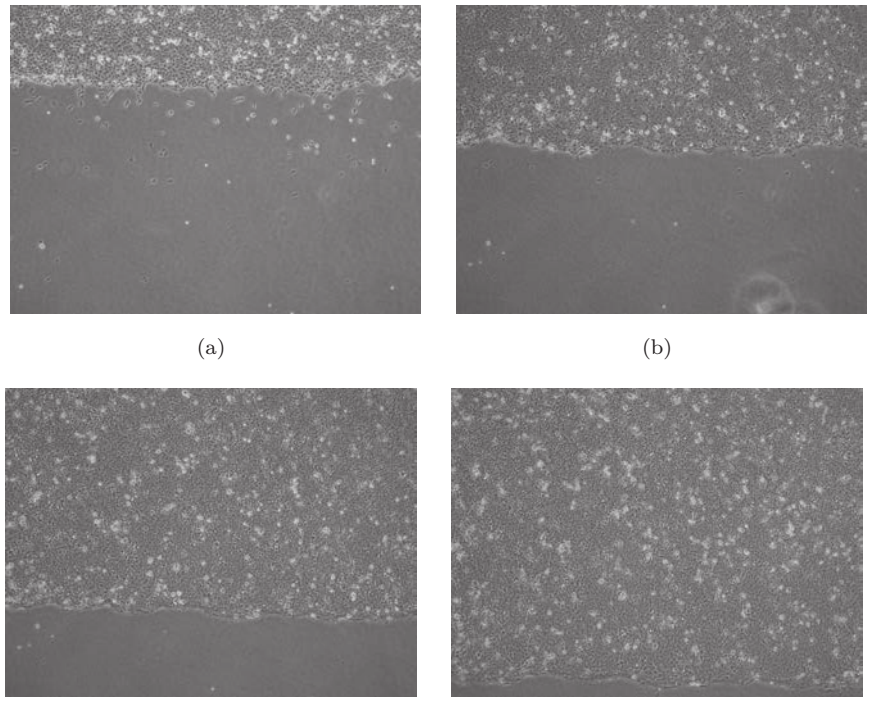

(a) (b)

(c) (d)

Figure 2.11: Timelapse at normal conditions. 2.11(a) at t= 0h, 2.11(b) at t= 16h, 2.11(c) at t= 33h and 2.11(d) at t= 50h,

because it will keep moving indefinitely while cells have enough nutrients. To better understand the cause of these behaviours we explore the spatio-temporal evolution of the velocity and cell density inside the monolayer, in the region near to the edge.

Figure 2.13 shows the distribution of the strip-averaged velocity for a representative experiment of set N (panel 2.13(a)) and another one of set S (panel 2.13(b)) at different depths (corresponding to different colors). Initially, the shallower cell layers develop the same speed in both sets (about 0.6 μ/min in these conditions). In set N, at the time when leading edge disappears from the field of view, not only cells close to the edge but also those at further distances exhibit a measurable velocity, albeit the fastest cells are found at the front. In other words, the velocity decays slowly with depth. However, in set S the velocity is zero everywhere, quite a lot of time before the edge arrives to the

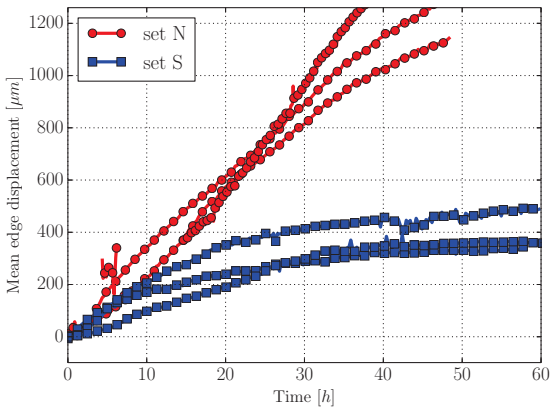

Figure 2.12: Time evolution of the leading edge for experiments at 10% (set N) and 1% (set S) of serum. Whereas experiments belonging to set N do not stop during the length of the experiment, starved cells (set S) stop well before this happens.

end of the field of view, consistently with the null advance velocity of the front.

At the layers far away from the edge, information of movement has not arrived, the signal is damped as it travels throughout the monolayer until its value is of the same order as noise levels. This result agrees with the model proposed by [20], where dashpots connecting cells to the substrate may weaken the forces transmitted inwards the monolayer, that will also diminish the velocity of the cells.

In contrast with the very different velocity distributions exhibited by cells in sets N and S, the evolution of the density profiles is qualitative identical. Figure 2.14 displays the density as a function of time for the same depths shown in figure 2.13. It can be appreciated how the difference between the density near the edge and that of the deepest layers measured (at about 1 mm from the front) is nearly kept constant throughout the experiment ($\Delta\rho \approx 600$ cells/mm). This conclusion is illustrated in a more quantitative way in figure 2.15, where the density is plotted as a function of the depth for the last image acquired in each experiment. Quite remarkably, the final density distribution is roughly the same in all cases, regardless of the serum concentration. Indeed, panel 2.14 shows the average of these density-depth curves performed for sets N and S separately, along with the maximum deviation with respect to the average, represented by the shaded areas. Observation of this figure reveals that, within

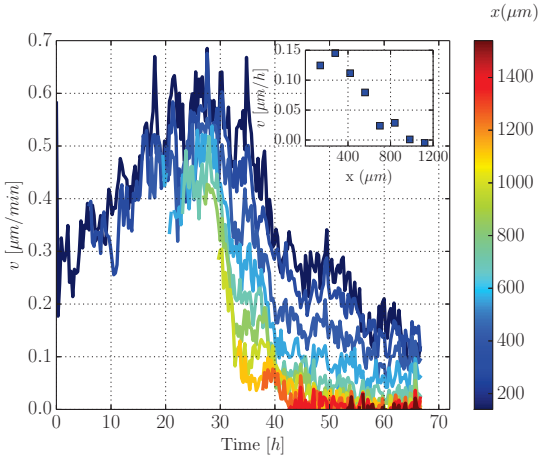

(a) Velocity at 10%FBS (set N)

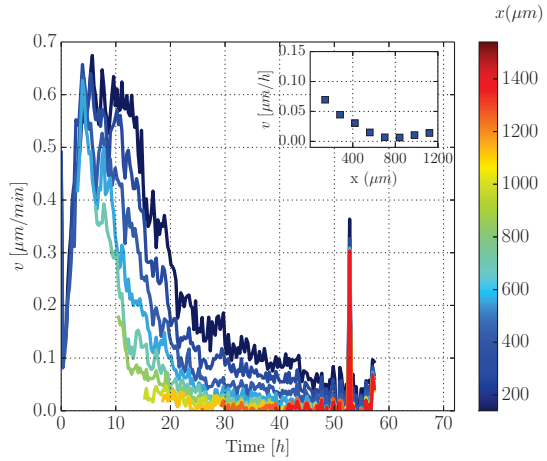

(b) Velocity at 1%FBS (set S)

Figure 2.13: Cell velocity normal to the edge for serum concentrations of 10% (set N) and 1% (set S). Insets show the velocity profiles as a function of the distance to the edge for the last time step (∼2700 min for set N and ∼ 3600 min for set S).

the variability observed in the experiments, both averages coincide near the edge. In fact, the maximum deviation of the curves with respect to the average of the two sets (black curve) is always smaller than ±20 %, a small variation taking into account that the density far from the edge almost doubles that at the front.

Since we are not able to capture a large fields of view nor mosaics we took consecutive images of the monolayer before and after the experiment to obtain long distance distribution of the density. In figure 2.15 the average initial and final density profiles if both experiments, starvation and normal conditions, is shown. Initially, the monolayer acquires almost constant density due to contact inhibition, this density is known as the carrying capacity of the monolayer. After three days, density near the advancing front has decreased but far from it the density remains the same and equal to the initial.

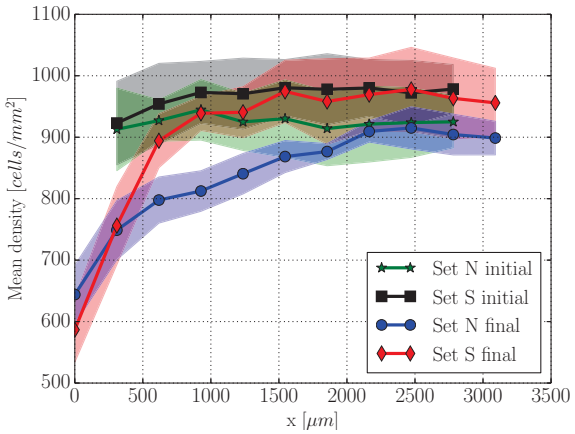

Figure 2.15: Initial and final density for several experiments for both cases, 1% and 10% of serum. They show a similar distribution with the depth in the monolayer and means

We carried out a two-tailed statistical analysis of the initial and final averaged density data among the experiments. Comparing the initial densities of set N and set S, we obtained a p-value= 0.7462, so we do not reject the null hypothesis of equal means at 5% of significance level. Performing the same analysis for final density distributions we get that p-value= 0.7662, which again leads to the conclusion that both profiles have the same mean.

In order to check that cell proliferation was indeed decreased in those exper-

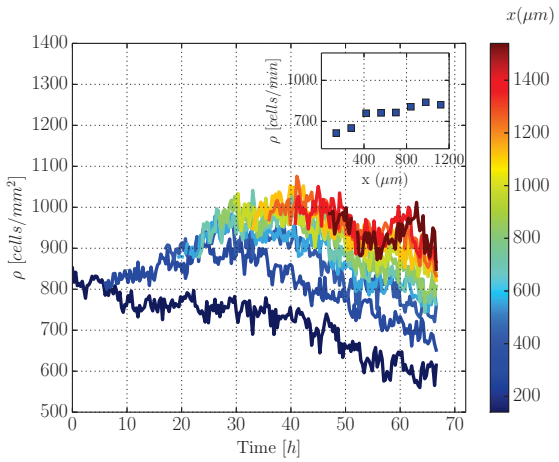

(a) Representative experiment for set N at 10% of serum

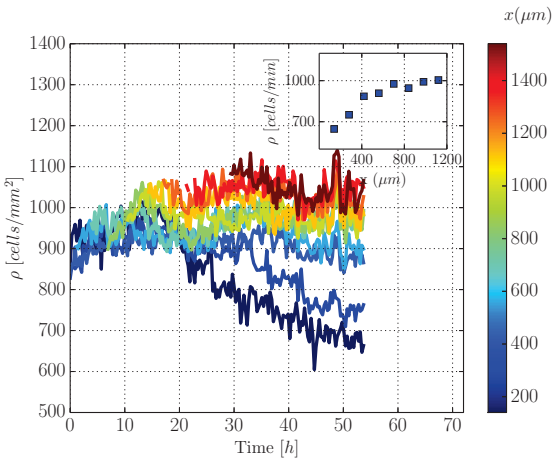

(b) Representative experiment for set S at 1% of serum

Figure 2.14: Density for two representative experiments of sets N and S, 10% and 1% serum concentration, respectively. Curves from set 1 end earlier before because the defect was already closed contrarily to set S. The reddish, the closer to the edge, the yellowish, the further from it.

iments carried out in starvation we performed a BrdU labelling at the beginning and at the end of the experiments as a tool to check that the number of proliferating cells was decreased and that the amount of apoptotic cells was not enlarged.

In figure 2.16 dividing cells were labelled following the protocol described in Materials and Methods section for BrdU stainning.

In figures 2.16(a) and 2.16(c) cells in S-phase of the cell cycle are labelled in green with BrdU and nuclei are marked in blue with DAPI. High percentage of proliferating cells are found in both cases, starvation and normal conditions, although in the first case proliferation should be inhibited. It looks like cells have memory or some inertia since they have been subjected to this inhibition for 24 hours before the experiment started.

In contrast, in figures 2.16(b) and 2.16(d), 72h after the experiment started cells were fixed and also labelled with BrdU. In this case, the percentage of proliferating cells in the monolayer in starvation had decreased significantly. This could be mainly the reason of the stop in movement of the cells, the lack of required nutrients for DNA replication. Since there is no proliferation the monolayer is not able to cover the free surface just by stretching itself.

In order to observe any difference in morphology of the cells regarding their ability to proliferate, we labeled the F-actin at the end of the experiment to check if cells were submited to the same strech.

Figure 2.17 show the pictures of f-actin staining after 72 hours of migration for the two cases under study, normal and starvation conditions, to investigate possible differences on cells cytoskeleton organization withing the monolayer.

2.4 Discussion

In this study, joint examination of figures 2.13 and 2.14 suggests that, when the region near the front monolayer advances, the region near the front adopts a fixed “advance formation” in the density profile. This formation is maintained until the monolayer either stops or closes the gap, depending on the serum concentration. Interestingly enough, this density distribution seems to be the same in all the experiments, and that seems to be unaffected by the monolayer speed, even when this is zero. Although the number of experimental conditions explored in this work is somewhat limited to assess the universality of this density distribution, the idea of a universal advance formation is very suggestive and will be tested in future experiments performed under a broader range of

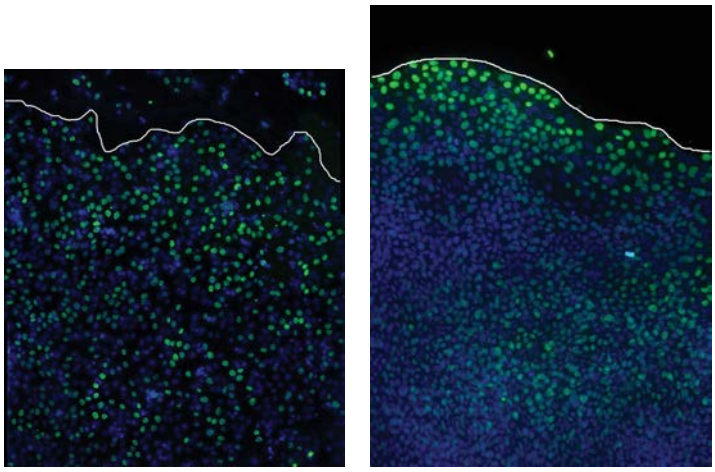

(a) Initial BrdU proliferation for set N

(b) Final BrdU proliferation for set N

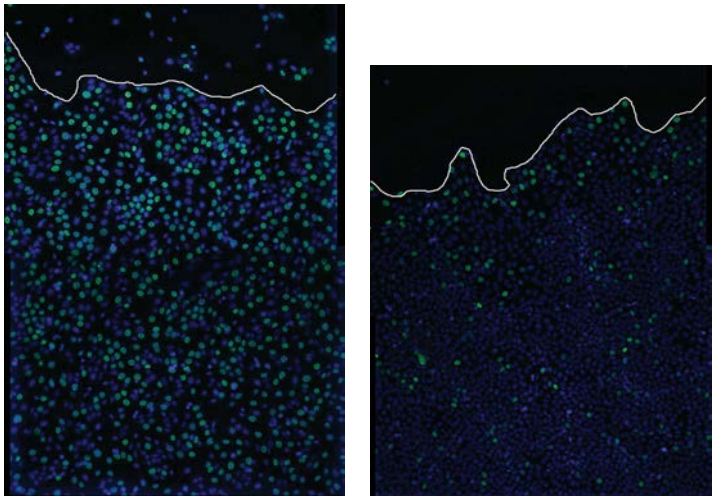

(c) Initial BrdU proliferation for set S

(d) Final BrdU proliferation for set S

Figure 2.16: Initial and final BrdU staining at the beginning and at the end of the experiment for set N and set S. Plot as a white line the edge of the monolayer

conditions.

A second conclusion directly follows from these observations: cell velocity

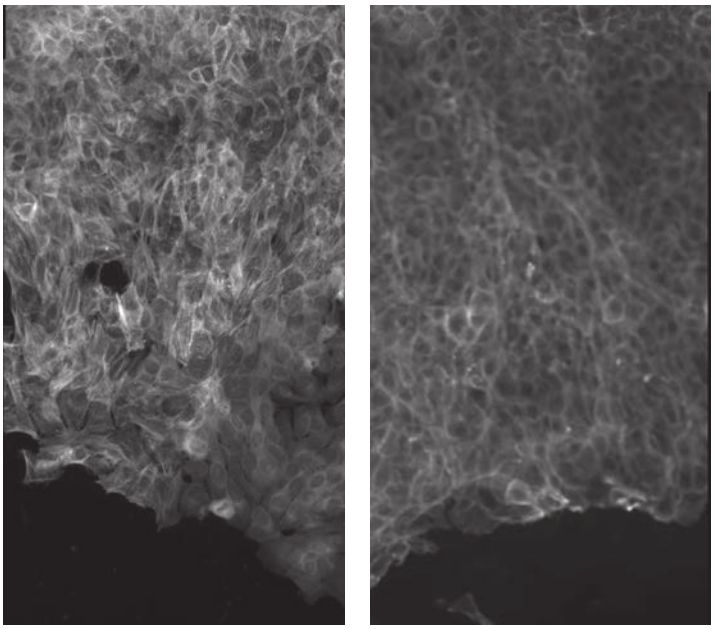

(a) F-Actin staining for set S at the end of the experiment

(b) F-Actin staining for set N at the end of the experiment

Figure 2.17: Final F-Actin staining at the end of the experiment for set N and set S.

does not uniquely depend on the local density, as it is assumed in a number of mathematical models of collective cell migration that hypothesize that the velocity of an individual cell is given by local density gradients [1]. Indeed, cells can even not move and still sustain the same density distribution. Consequently, in order to properly model the behaviour of the cell monolayer at a particular time, the time history needs to be taken into account.

Since the distribution of the density within the monolayer at the end of the experiment is quite similar between among all cases, whether the gap is closed or not. This is a clear evidence that the density is not driving the population of cells. Density might be considered given by an universal distribution or "advance formation". It is kept even when cell migration stops. This behaviour is contrary to the hypothesis that the velocity is function of the cell density.

Finally, two inmunestainning were performed, to label proliferating cells and the f-actin filaments. In the first case, at the beginning of the experiment there was no significant difference between starvation and normal condition number

of proliferating cells. Instead, after 72 hours experiment at 1% of FBS barely showed proliferating cells in contrast to the experiment at 10% of FBS that kept the number of proliferating cells similar to the initial values. One of the most interesting aspects in this results is that the assays did not display spatial distribution of division since we expect to see more proliferating cells far from the edge. On the other hand, we perform the stainning of F-actin filaments in order to see if there was any significant difference in actin polimerization or distribution between the two cases. We observed that actin is polimerized in the trailing edge over several cell rows, further from this length it is located at the cell contour as in confluency. This suggests that cells far from this length scale do not feel the stresses created by the symmetry break in the edge.

Nomenclature

ABM	Agent Based Models
PIV	Particle Image Velocimetry
BrdU	Bromodeoxyuridine
DMEM	Dulbeco's Modified Eagles Medium
FBS	Fetal Bovine Serum
PBS	Phosphate Buffer Serum
PDMS	Polydimethylsiloxane
UV	Ultraviolet
DNA	Deoxyribonucleic acid
BSA	Bovine Serum Albumin
HCl	Clorhidric Acid
DAPI	4 ',6-diamino-2-fenilindol
FFT	Fast Fourier Transform

Bibliography

[**1**] B. M. H. D. Arciero J.A., Mi Q. and S. D. Continuum model of collective cell migration in wound healing and colony expansion. *Biophysical Journal*, 100:535:543, 2011.

[**2**] R. A. C. W. S. at San Diego State University. Marker-Controlled Watershed Segmentation. URL www.rohan.sdsu.edu.

[**3**] W. J. N. Daniel J. Cohen and M. M. Maharbiz. Galvanotactic control of collective cell migration in epithelial monolayers. *Nature Materials*, 13: 409–417, March 2014.

[**4**] T. E. A. K. R. C. Y. P. . X. S.-P. E. H. Z. M. H. Z. J. P. B. D. A. W. J. J. F. Dhananjay T. Tambe, C. Corey Hardin and X. Trepat. Collective cell guidance by cooperative intercellular forces. *Nature Materials*, 10:469–475, June 2011. doi: DOI:10.1038/NMAT3025.

[**5**] K. P. W. H.P.Ng, S.H.Ong. Medical image segmentation using k-means clustering and improved watershed algorithm. *IEEE*, page 61:65, 2006.

[**6**] B. A.-L. J. R.-R. A. A. R. A. F. Juan C. del Alamo, Ruedi Meili and J. C. Lasheras. Spatio-temporal analysis of eukaryotic cell motility by improved force cytometry. *PNAS*, 33:13343âĂŞ13348, August 2007.

[**7**] K. Y. S. J. Khammanit R., Chantakru S. Effect of serum starvation and chemical inhibitors on cell cycle synchronization of canine dermal fibroblasts. *Theriogenology*, 70:27:34, 2008.

[**8**] O. C.-E.-B. L. A. B. S. C. F. A. J. C. M. Reffay, M. C. Parrini and P. Silberzan. Interplay of rhoa and mechanical forces in collective cell migration driven by leader cells. *Nature Cell Biology*, 16:217–223, February 2014.

[**9**] J. P. T. W.-B. R. G. T. F. W. A. G. P. W. . Y. G. . T. S. . A. S. . J. V. F. . H. R. B. P. N. D. C. D. M. Min Zhao, Bing Song and J. M. Penninger. Electrical signals control wound healing through phosphatidylinositol-3-oh kinase- g and pten. *Nature Letters*, 442:457–460, July 2006.

[**10**] R. P. and M. D.S. Cell density determines epithelial migration in culture. *Proc. Natl. Acad. Sci.*, 77:4760–4763, 1980.

[**11**] P. Roth. Collective cell migration. *Annual Review of Cell and Developmental Biology*, 25:407:429, 2009.

[**12**] J. C. d. A. R. A. F. Ruedi Meili, Baldomero Alonso-Latorre and J. C. Lasheras. Myosin ii is essential for the spatiotemporal organization of traction forces during cell motility. *Molecular Biology of the Cell*, 21:405–417, February 2010.

[**13**] B. L. O. C. B. L. H. D.-A. F. G. S. Tlili, E. Gauquelin. Waves in cell monolayer without proliferation: density determines cell velocity and wave celerity.

[**14**] X. T. M. M. J. J. F.-a. D. A. W. Thomas E. Angelini, Edouard Hannezo. Glass-like dynamics of collective cell migration. *PNAS*, 12:4714:4719, 2011.

[**15**] A. Tremel, A. Cai, N. Tirtaatmadja, B. Hughes, G. Stevens, K. Landman, and A. OâĂŹConnor. Cell migration and proliferation during monolayer formation and wound healing. *Chemical Engineering Science*, 64(2):247 – 253, 2009. ISSN 0009-2509. doi: http://dx.doi.org/10.1016/j.ces.2008.10.008. URL http://www.sciencedirect.com/science/article/pii/S0009250908005356.

[**16**] A. T. M. E. W. D. B. J. Trepat .X, Wasserman M.R. and F. J.J. Physical forces during collective cell migration. *Nature Physics*, 5:426:430, 2009.

[**17**] L. C. Vedula E.R.K., Ravasio A. and L. B. Collective migration: a mechanistic perspective. *Physiology*, 28:370:379, 2013.

[**18**] P. Vitorino and T. Meyer. Modular control of endothelial sheet migration. *Genes Dev.*, 22:3268–3281, 2008.

[**19**] T. W. and S. E.J. Pivlab- time-resolved digital particle image velocimetry tool for matlab. 2014.

[**20**] R. V. E. A. D. T. T.-E. B. J. P. B. J. J. F. Xavier Serra-Picamal, Vito Conte and X. Trepat. Mechanical waves during tissue expansion. *Nature Physics*, 8:628–634, 2012.

[**21**] X. L. J. Q. C. T. Yu Wang, Guixue Wang. Substrate stiffness regulates the proliferation, migration, and differentiation of epidermal cells. *Burns*, 38:414:420, 2012.

CHAPTER
THREE

Continuum model of cell monolayer migration

Contents

3.1 Introduction

Mathematical models have been developed to test some hypotheses related to how cell migration occurs in wound closure. Here we are summarizing those ones we are interested in due to the nature of their assumptions and application.

Agent-based models (ABM) [5] simulate cell migration where cells respond to crowded conditions by decreasing proliferation and migrating to less crowded areas.

In [1] they have developed a two-dimensional continuum mechanical model of a migrating cell sheet that describes the elastic coupling between cells in the layer, the adhesion of cells to the substrate, the force generated by lamellipodia and the proliferation. Cell sheet is represented as a compressible inviscid fluid(individual cells are indistinguishable).

There are other continuum models of cell migration in wound healing based on reaction-diffusion formulation [3] where the cell population is described as a travelling wave (Fisher equation). This equation describes the cell density, where the cell motility is prescribed by a diffusive flux (diffusion coefficient is a function of cell density). With the individual cell trajectory data, contact inhibition effect is quantitatively determined and its effect on migration. They developed a multi-scale model approach to analyse population-scale behaviour and the individual cell-scale function in wound-healing assay. In that way, they compare the different results and are able to validate the estimated parameters present in the model.

There are other models, as well based on Fisher-KPP equation, such as [4]. In this case, they have studied two different situations, activated and inhibited migration conditions They showed that for some migration assays cell dynamics cannot be described by Fisher-KPP equations.

Both models, [4] and [3], are mainly based on density variations in the monolayer, that is to say the diffusivity of cells in the monolayer during the wound closure.

Another explanation of collective movement of thousands of cells is given in [6]. They have modelled the displacement of cells in a collective way describing cells as point particles with a dynamic based on 1: cells move in a stochastic manner and 2. tend to adapt their motion to that of their neighbours.

There is also a 3D model created by [9] where they have developed a simplified finite-element model that takes into account the sequential steps of wound healing. The model is a nonlinear coupled diffusion-reaction and visco-elastic equations. In this case, motility is generally represented by a diffusive flux where diffusion coefficient is a function of density and concentration of chemicals.

Our methodology consists of image processing of video sequences of a given migration assay in order to obtain spatio-temporal information of density and displacements. The latter inferred from interpolated velocity fields from PIV analysis. With this data we fitted the free parameters of the model that we were not able to directly measure from our experiments. Then we compared obtained density and displacements profiles to check whether the model works or fail to reproduce in vitro data. Finally we study the influence of the parameters on the convergence of the model finding that not all of them were needed to get the same result.

3.2 Continuum models formulation

Our goal is not to develop a completely new mathematical model but use the terms or equations already published that would fit better our experimental findings. First, it is essential to explain the models found in the literature to understand our results and the relations between velocity and density. There are different models proposed by the authors and they stablish diverse relations between the velocity and the density.

In [4], they propose a diffusion model based on Fisher-KPP equation with a linear-growth term.

$$\frac{\partial \rho}{\partial t} = D\Delta\rho + r\rho(1-\rho) \tag{3.1}$$

In the equation 3.1 , ρ is the relative density (cell density/ cell density at confluence) at position x=(x,y) and time t, r is the linear growth rate, and the parameter D is the diffusion coefficient. The velocity of the wave front is assumed to be constant.

They carried out different assays to compare computational results to experimental data. The control dynamics were accurately predicted by the model but accelerated and inhibited migration experiment behaviours were not well captured in many cases.

The model proposed by [3] goes a bit further introducing a diffusivity parameter that takes into account the contact inhibition effect in the movement. Besides, they insert a logistic growth term instead of a linear one and non-dimensionalize the problem arriving to equation 3.2.

$$\frac{\partial \rho}{\partial t} = \frac{\partial}{\partial \xi}\left(D(\rho)\frac{\partial \rho}{\partial \xi}\right) + \rho(1-\rho) \tag{3.2}$$

The diffusivity function D(u), is modelled considering the contact inhibition of locomotion that takes into account that the increase in density, decreases the movement and besides, the diffusivity. The solution of this equation are the Fisher equation travelling waves with the minimum wave speed. They apply a continuum model to obtain the diffusivity in crowded conditions and at low densities to understand the contact inhibition effect. This is not considered in the original Fisher equation, that is the reason of introducing a non-linear diffusion coefficient. They also apply a discrete model to probe the existence of differences between cells at the wavefront and cells behind it. Fisher equation is

not able to capture those difference at cell level behaviour and does not match with experimental data, but, the model that includes the contact inhibition effect in diffusivity exactly reproduces it.

By contrast, [1] proposes a continuum mechanical model based on the elastic deformation of the layer.

$$\frac{\partial \rho}{\partial t} + \nabla(\rho \mathbf{v}) = \mathbf{g}(\mathbf{u}) \tag{3.3}$$

In 3.3, $\mathbf{v}$ stands for the velocity of the leading edge. The Laplacian appears in 3.3 from constitutive equations, not from diffusion of Brownian motion. That's why k should not be considered as a diffusion coefficient. Besides, they neglect the logistic growth term (g(u)) in the free boundary layer problem, that corresponds to wound healing.

In [9] proposes a 3D model that could be also considered for the 2D problem studied here.

$$\frac{\partial \rho}{\partial t} = \frac{\partial}{\partial x}\left(-D_\rho \frac{\partial \rho}{\partial x} + D_c(\rho, c)\frac{\partial c}{\partial x}\right) + r\rho\left(1 - \frac{\rho}{\rho *}\right) - d_\rho \rho \tag{3.4}$$

In 3.4 D_ρ is the diffusion or motility coefficient while D_c stands for the amount of cells that diffuse a concentration gradient of a chemical. c is the concentration of chemicals, such as growth factors. $\rho*$ is the saturation or the carrying capacity of cell density and $d_\rho\rho$ is the death term rate. They solve this equation for a 3D problem but it could be used for the monolayer.

Finally, there is a completely different model proposed by [6] where the displacement of each cell is patterned by considering the movement of individuals as stochastic and they tend to adapt it to the collective motion.

$$\frac{\partial v_i}{\partial t} = -\alpha v_i + \sum\left[\frac{\beta}{N_i}(v_j - v_i) + f_{ij}\right] + \sigma(\rho_i)\eta_i \tag{3.5}$$

In 3.5 v_i is the velocity of the cell i. $-\alpha v_i$ is a linear damping term. f_{ij} is the force between cells i and j. β is the strength between cells and σ is the noise.

A different model proposed by the same group [7], is a physical model of the cell migration during wound healing but considering that the monolayer expands in a non-uniform way developing finger-like shapes at the edge. The culture interface is modelled as a membrane described by a Helfrich energy functional with bending and surface tension terms. Also, the forces produces

by the cells are included: internal force due to cellular motility, normal restoring force and noise due due to random velocity(as they proposed in [6]. Finally they arrive to the equation for the motion of the leading edge. This model is just focused on understanding the mechanisms in the finger. We are more interested in a deeper analysis of the tissue.

$$\frac{\mathrm{d}\mathbf{r}}{\mathrm{dt}} = -\frac{\mathrm{k}}{\eta}\frac{\partial^2 \mathbf{H}}{\partial \mathrm{s}^2} + \frac{\gamma}{\eta}\mathbf{H} - \frac{\mathbf{3k}}{\mathbf{2h}}\mathbf{H^3} + \frac{(\mathbf{F_{cell}} + \mathbf{F_r})\widehat{\mathbf{n}}}{\mathbf{h}} + \mathbf{n}\widehat{\mathbf{n}} \tag{3.6}$$

They analyse the instabilities of the equation which produces the finger form at the edge and the influence of the various parameters present in the model. The chemical and mechanical signalling is proposed to be included in future works.

According to [8] there is a mechanism that establishes a long-range cell guidance in the tissue, that is that the coherent movement in the monolayer penetrates long distances or several strips of cells behind the leading edge.

3.3 Mathematical formulation of the model

In this study, we propose the combination of the models proposed by Banerjee and Arciero ([2] and [1]) that will reproduce the biological processes we observe in experiments. We mainly use the equations established by Banerjee [2] but replacing the propulsion force by the pressure term as a function of the density gradient suggested by Arciero [1]. Arciero [1] proposed a model that captures the motion of the cell sheet, particularly, the elastic coupling between cells, the cells adhesion to the substrate, force generated within the monolayer and proliferation, applied to different wound geometries.

3.3.1 Equations of the model

Banerjee et al. [2] proposed a continuum model for the spreading of a cell monolayer represented as an elastic continuum medium coupled to the concentration of active contractile units. The model is able to reproduce stress propagation based on the local feedback between elastic deformations and cell contractility. Here we show an schematic representation of the geometry of the model (figure 3.1).

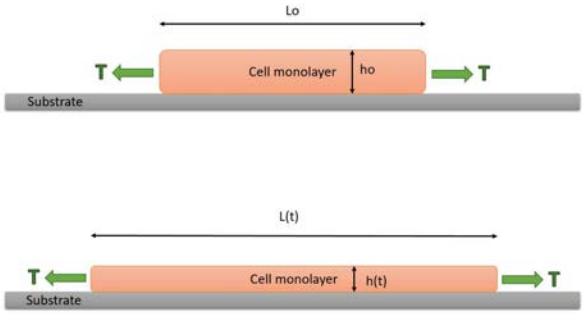

Figure 3.1: Scheme of the geometry of the cell monolayer modelled according to Banerjee model [2]

The equation of the motion governing the displacement field, u(x,t), of the cell monolayer (figure 3.1) is:

$$\Gamma \partial_t u = f_0 p(x,t) + h(t)\partial_x \sigma \tag{3.7}$$

where $\sigma(x,t)$ is the internal stress in the monolayer given by the sum of the internal pressure(Π), an elastic stress composed by the compressional elastic modulus B and the strain field ($\varepsilon = \partial_x u$) and the active stress σ_a that is function of the contractile units, such as phosporylated myosins interacting with actin fibers.

$\sigma = -\Pi + B\varepsilon + \sigma_a(c)$

Π is a constant pressure that appears due to the internal growth when cells proliferate. The active stress σ_a is proportional to the logarithm of the concentration of species.

$\sigma_a(c) = \beta \log(c/c_0)$

considering that c_0 is the concentration of contractile elements at equilibrium ($f_0 = 0$) and $\beta > 0$.

The dynamics of the concentration field $c(x,t)$ is given by:

$$\partial_t c = -\frac{1}{\tau}(c - c_0) + \alpha\varepsilon - \partial_x J \tag{3.8}$$

τ is the time scale of the turnover of the contractile elements, $\alpha > 0$ is the rate of production of $c(x,t)$ due to local extension and J(x,t) is the current of transport of active units. The total current is the sum of diffusive and convective fluxes:

$J = -D\partial_x c + c\partial_t u$

where D is the diffusion constant.

Banerjee et al. [2] consider a constant propulsive force at the wound edge of the form of:

$p(x,t) = \tanh(x/\lambda)$

This constant force pulling at the edge is very strong, poorly phisiological and makes the tissue unable to adapt to it. We seek a more realistic expression for the mechanism that is driving the movement. For this reason, we consider Arciero et al. [1] concept of pressure would fit better the results observed during our experiments. This internal pressure depends on cell density providing an expression that relates velocity of cells with cell density gradient.

$p(\rho) = k \cdot \log(\rho/\rho_0)$

where ρ_0 is the initial and homogeneous density.

Since this term introduces a new variable in the problem the formulation of an additional equation is needed. We then add to the system the continuity equation in order to assure that the cell number is conserved.

$$\partial_t \rho + \partial_x(\partial_t u \cdot \rho) = g(\rho) \tag{3.9}$$

We study the case without proliferation, setting the source term $g(\rho)$ in equation 3.9 equals zero, since the spatiotemporal generation of new cells remain unknown for us.

We finally obtain the final set of equations to be solved(3.11, 3.12 and 3.10) that define the dynamics of the spreading monolayer, together with their boundary and initial conditions:

$$\partial_t \rho + \partial_x(\partial_t u \cdot \rho) = 0 \tag{3.10}$$

$$\Gamma\partial_t u = -k\partial_x\left(\ln\frac{\rho}{\rho_0}\right) + h(t)\cdot\partial_x\left(-\Pi + B\partial_x u + \beta\ln\left(\frac{c}{c_0}\right)\right) \tag{3.11}$$

$$\partial_t c = -\frac{1}{\tau}(c - c_0) + \alpha\partial_x u + D\partial_x^2 c - \partial_x c\partial_t u - c\partial_x(\partial_t) \tag{3.12}$$

Then we establish the boundary and initial conditions of the problem.

The boundary of the monolayer is stress-free:

$$\sigma(\pm L/2, t) = 0 \tag{3.13}$$

Initially the monolayer is undeformed:

$$u(x,0) = 0 \tag{3.14}$$

Initial homogeneous concentration of contractile elements:

$$c(x,0) = c_0 \tag{3.15}$$

No flux of active units:

$$\partial_x c(\pm L/2, t) = 0 \tag{3.16}$$

Initial homogeneous cell density in the monolayer:

$$\rho(x,0) = \rho_0 \tag{3.17}$$

The length of the monolayer or the position of the advancing edge is determined as:

$$L(t) = L_0 + u(L_0/2, t) - u(-L_0/2, t) \tag{3.18}$$

Height of the monolayer is determined by volume conservation since there is no proliferation:

$$h(t) = \frac{h_0 L_0}{L(t)} \tag{3.19}$$

where h_0 and L_0 is the initial size of the monolayer, as is shown in figure 3.1.

3.3.2 Dimensionless problem

We obtain the following nondimensional variables with the chosen scaling parameters:

$$U = u/u_c; \quad T = t/t_c; \quad R = \rho/\rho_0; \quad X = x/L; \quad C = c/c_0$$

Then, to rearrange the equations in terms of the nondimensional variables we need to redefine the derivatives:

$$\frac{\partial}{\partial t} = \frac{\partial T}{\partial t}\frac{\partial}{\partial T} + \frac{\partial X}{\partial t}\frac{\partial}{\partial X} = \frac{1}{t_c}\frac{\partial}{\partial T} + \frac{-L'}{L^2}x\frac{\partial}{\partial X} = \frac{1}{t_c}\frac{\partial}{\partial T} - \frac{l'}{l}\frac{X}{t_c}\frac{\partial}{\partial X} = \frac{1}{t_c}(\partial_T - \frac{l'}{l}X\partial_X)$$

$$\frac{\partial}{\partial x} = \frac{\partial X}{\partial x}\frac{\partial}{\partial X} = \frac{1}{L_0 l}\frac{\partial}{\partial X}$$

$\frac{\partial^2}{\partial x^2} = \frac{1}{L_0^2 l^2}\frac{\partial^2}{\partial X^2}$

Now, we substitute above expressions into equations 3.11, 3.12 and 3.10 leading to the following dimensionless set of equations with their corresponding initial and boundary conditions.

$$\partial_T R - \frac{l'}{l} X \partial_X R + \frac{u_c}{L_0}\frac{\partial_X}{l}(R(\partial_T U - \frac{l'}{l} X \partial_X U)) = 0 \tag{3.20}$$

$$\partial_T U - \frac{l'}{l} X \partial_X U = V = -\frac{1}{l}\partial_X(\log R) + \frac{1}{l^3}\partial_X\left(\bar{B}\partial_X U + \bar{\beta}\log C\right) \tag{3.21}$$

$$\partial_T C - \frac{l'}{l} X \partial_X C = -\frac{1}{\tau}(C-1) + \bar{\alpha}\frac{1}{l}\partial_X U \bar{D}\frac{1}{l^2}\partial_{XX} C - \frac{1}{l}(\partial_X C V + \partial_X V C) \tag{3.22}$$

The new boundary conditions turns into:

$l' = \frac{2\partial_T U}{1+\frac{1}{l}\partial_X U}|_{X=1/2}$
No flux of active units:

$\partial_X C(\pm 1, T) = 0$
From free stress boundary condition:

$\bar{\beta}\partial_X U(\pm 1, T) = l(\bar{\Pi} - \bar{\beta}\log C)$
Initially monolayer is undeformed and has homogeneous density and concentration of contractile units:

$R(X, 0) = 1$
$C(X, 0) = 1$
This formulation leads to a set of six free parameters that need to be fit in order to meet our results from the experiments:

3.4 Interpolation of the displacement field from experiments

In order to obtain the displacement field along time in our experiments from PIV data we placed synthetic tracers that will move and evolve in time according

$\bar{D}$	$\frac{4D\tau}{L_0^2}$	Diffusivity of contractile units
$\bar{B}$	$\frac{4Bh_0\tau}{L_0^2\Gamma}$	Elasticity-friction rate
$\bar{\beta}$	$\frac{2\beta h_0\tau}{L_0\gamma u_c}$	Reinforcement-friction rate
$\bar{\alpha}$	$\frac{\alpha u_c\tau}{L_0}$	Recruitment
$\bar{\Pi}$	$\beta \cdot 10^{-3}$	Internal pressure
$\bar{\tau}$	$\frac{t_c}{\tau}$	Time scale of turnover of the contractile elements

Table 3.1: Table of free dimensionless parameters to be fitted

to interpolated velocity based on Euler displacement.

$$Xp(t) = Xp(t-1) + Vp \cdot \Delta t$$

Vp is the interpolated velocity using Biharmonic Spline Interpolation already implemented in MatLab. This algorithm is suitable for nonuniformly spaced data and fits the point particles to the surface defined by the velocity field at each time.

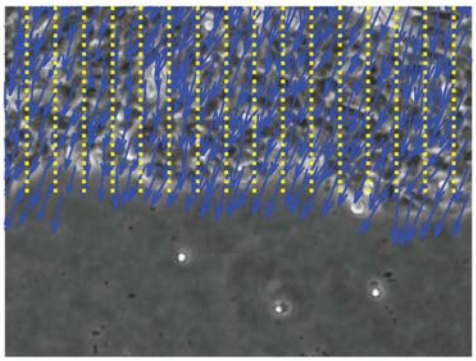

Figure 3.2: Initial position of the tracers forming a 2D grid and the velocity field

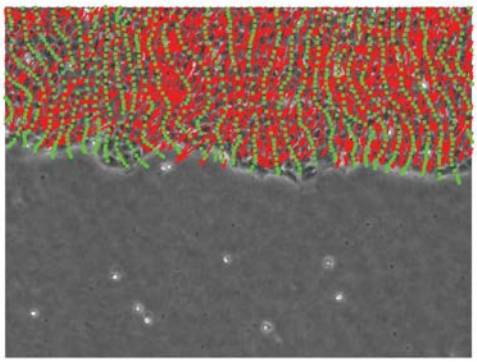

Figure 3.3: Position of the tracers that have evolved according to the interpolated velocity field

In figure 3.2 the initial uniformly distribution of the particles is shown and some time later, in figure 3.3, the particles have evolved according to the interpolated velocity.

3.5 Parameter fitting

The problem consists on solving a system of three partial differential equations with six free unknown parameters.

In order to find the most adjusted values of the parameters we first look at the temporal evolution of the edge.

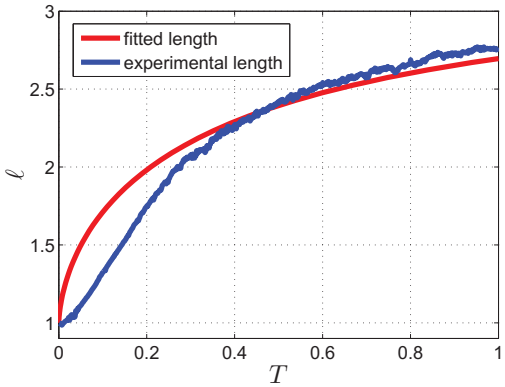

Figure 3.4: Experimental and numerical length of the domain.

In order to obtain a set of parameters to solve the numerical problem we use the the curve of the temporal evolution of the edge to be fitted (figure 3.4). Then, with the set of parameters that minimizes the error we solve the numerical problem that leads to the final displacement profile.

$\bar{D}$	1.3757
$\bar{B}$	0.0002
$\bar{\beta}$	0.0275
$\bar{\alpha}$	188.1249
$\bar{\Pi}$	20.0139
$\bar{\tau}$	0.6831

Table 3.2: Table of free dimensionless parameters obtained thorugh l(t) fitting

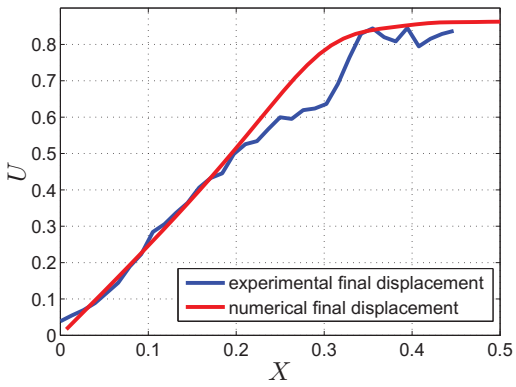

Figure 3.5: Experimental and numerical final displacements.

Figure 3.5 shows that the chosen parameters suits the final displacement profile obtained through the temporal evolution of the tracers interpolated from the velocity field from PIV.

Finally, we can see if the fitting to the length of the tissue also provide a good agreement in density proliles, which is the other variable we are able to quantify experimentally.

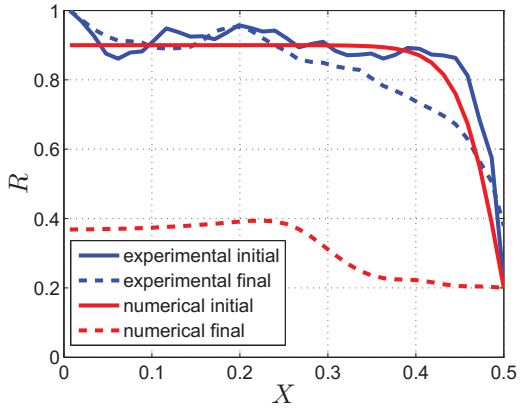

Figure 3.6: Experimental and numerical initial and final density profiles.

In contrast to displacement field within the tissue and the border enlargement, density is not well capture by the model. We require a thin layer to stretch, without proliferation, alost three times its initial size. The density has to decrease a lot to achieve this condition.

Since the total size of our tissue is not the initial length we observe in the field of view at the beginning of the experiment (around 600µm) but half of a petri dish which radius is close to 17000µm, we set initial length to this value and solve the problem again.

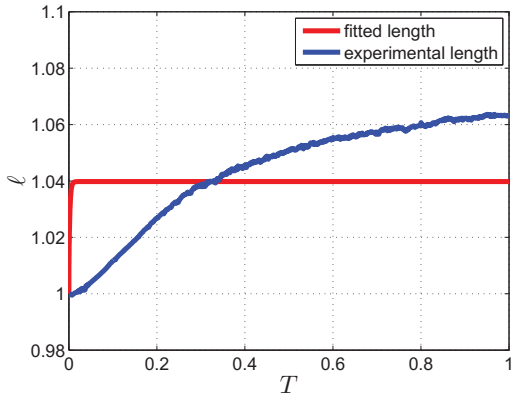

Figure 3.7: Experimental and numerical length of the domain.

When we set the real size of the tissue the monolayer becomes very stiff and cells far away front the edge do not sense any gradient so they do not move

at all. The model is not able to propagate information or forces at very long distances because it does not behave as a spring.

$\bar{D}$	43.9319
$\bar{B}$	0.3544
$\bar{\beta}$	0.8049
$\bar{\alpha}$	3899.4
$\bar{\Pi}$	1816.1
$\bar{\tau}$	107.193

Table 3.3: Table of free dimensionless parameters obtained thorugh l(t) fitting when the size of he real domain is introduced.

According to the displacement curve, cells found far from the edge but close enough to be captured in the field of view, show a barely appreciable displacement. We set a threshold in the velocity, reducing the velocity of those points below that value, tipically far from the edge, so we reduce the spring behaviour the tissue is showing in the simulations results.

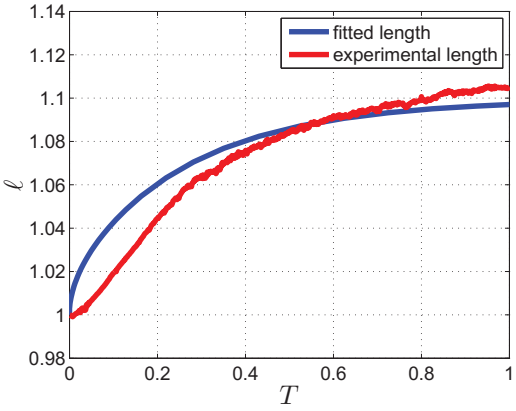

Figure 3.8: Experimental and numerical length of the domain setting a threshold velocity when real dimensions of the tissue is considered.

Now setting a threshold velocity the model is able to fit the length of the tissue, as shown in figure 3.8). The resulting parameters are displayed in the

following table.

$\bar{D}$	15.6169
$\bar{B}$	0.0018
$\bar{\beta}$	0.001
$\bar{\alpha}$	10.6673
$\bar{\Pi}$	9.215
$\bar{\tau}$	0.5389

Table 3.4: Table of free dimensionless parameters obtained thorugh l(t) fitting when the size of he real domain is introduced.

Once the parameters are obtained 3.4) the rest of the variables are computed.

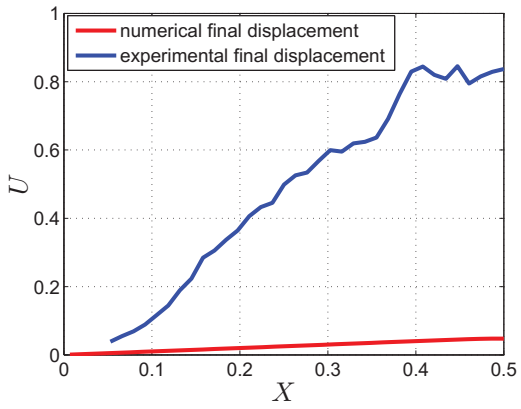

Figure 3.9: Final displacement profiles obtained numerically or interpolated from experimental velocity fields.

Although, now the temporal evolution of the edge (figure 3.8) is better captured, the final displacement field is not achieved (figure 3.9).

The other variable we are interested in is the density. The initial density profile is fitted to the experimental to stablish the same initial conditions, then we expect the model is able to recover the beahviour observed in the analysis.

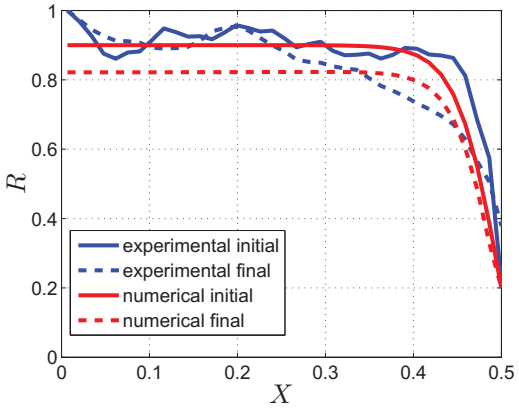

Figure 3.10: Experimental and numerical density setting a threshold velocity when real dimensions of the tissue is considered. Initial and final spatial density profiles are shown.

Although the velocity threshold helpped in the parameter interpolation fitting the length of the tissue, the spatial distribution of the final density is not properly obtained (figure 3.10).

The whole density has decreased and this phenomenon is more evident close to the edge but, far from the border the density do not keep the confluent density value,as the experiments. There is still a need of a boundary condition in the model forcing the density remain the same if cells are not moving.

Kymographs can be useful to compare spatio-termporal evolution of some variables such as the density from experiments and the results obtained from the numerical computation.

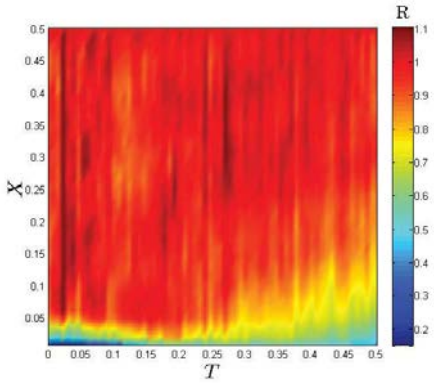

Figure 3.11: Spatio-temporal kymograph of the experimental density

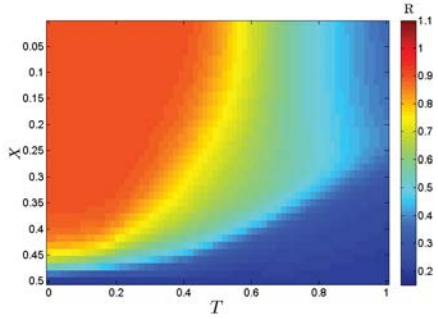

Figure 3.12: Spatio-temporal kymograph of the numerical density obtained for a small domain

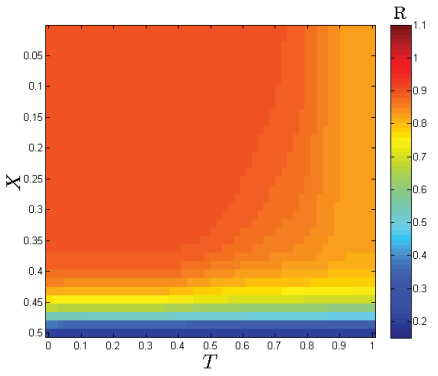

Figure 3.13: Spatio-temporal kymograph of the numerical density obtained for a big domain when a threshold velocity is introduced in the model.

The model is not working properly when the real dimensions of the tissue are addded. A new term modelling the friction of the tissue is needed. Until now this phenomenon was introduced simply as viscous friction and later with a threshold velocity limiting the spring-like beahaviour of the tissue. The intercellular stresses are transmitted without any damping to the whole monolayer. This kind of models are thougth to work on small domains like narrow strips of cells, small colony expansion or small defects.

3.6 Influence of parameters on the solution

In this section the influence of the free parameters is under study and as a consecuence, the importance of some terms in the equations if those parameters

are forced to zero.

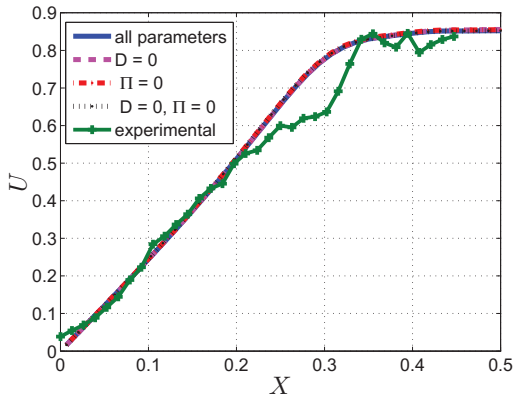

Figure 3.14: Parameter influence on the domain length fitting for a small domain.

Including all the parameters in the model, setting diffusivity to zero, cancelling the internal pressure or both at the same time shows no significant differences in the final displacement (figure 3.14). Besides, all of them are very similar to the experimental curve.

This curve is showing that several terms in the model are not necessary or at least are not contributing enormously in the solution.

We have observed that in spite of fitting quite well the length of the domain the model can still fail to meet other variables behaviour.

3.7 Discussion

In this chapter we have combined two models from the literature [1] and [2] that seem to show similar behaviours to ours observed during the experiments.

When we consider that the size of our domain, or tissue, is the observed length in the field of view, we can compute a parameters' fitting that seem to provide a good agreement in the temporal evolution of the length of the monolayer. Then, if we look at the final displacements profile it also show similar behavior compared to the interpolated displacements from the velocity fields. Finally, if we look at the other varible we are able to measure, the density, the model is not able to reproduce the final density profile. We are requiring the tissue to triple its size but without proliferation, then, to conserve the mass, the density has to decrease.

Then, if we set the length of the monolayer to its actual size that is half of the petri dish, 17000μm the results are completely different. The model is not able to fit the parameters to meet the lenght of the tissue. Then, the displacements and density are not comparable to experiments either.

Regarding the displacements, we observe that at certain distance from the edge cells barely show significant displacement. So we can introduce in the model a threshold velociy below which the displacements will be null. In this case, the parameter fitting again reproduce the general tendency of the length of the tissue.

In addition we have also investigate the influence of several parameters in the model and we have observed that the diffusion and the internal pressure do not play an important role in the model when fitting the length of the tissue.

As a general conclusion, this models work in reduced size systems since they stress are fully spread but in the case of a big monolayer the model fail to reproduce our results.

We will further explore the effect of the a friction term in the model to soften the effect of forces inwards the tissue. Then we will also study the problem considering a proliferation term in the continuity equation. Until now this case was not considered due to our inability to detect proliferating cells in time and space.

Bibliography

[**1**] B. M. H. D. Arciero J.A., Mi Q. and S. D. Continuum model of collective cell migration in wound healing and colony expansion. *Biophysical Journal*, 100:535:543, 2011.

[**2**] S. Banerjee, K. J. C. Utuje, and M. C. Marchetti. Propagating stress waves during epithelial expansion. *Phys. Rev. Lett.*, 114:228101, Jun 2015. doi: 10.1103/PhysRevLett.114.228101. URL https://link.aps.org/doi/10.1103/PhysRevLett.114.228101.

[**3**] L. K. Cai, A.Q. and H. B.D. Multi-scale modeling of awound-healing cell migration assay. *Journal of Theoretical Biology*, 245:576:594, 2007.

[**4**] M. G. Habbal A., Barelli H. Assessing the ability of the 2d fisher-kpp equation to model cell-sheet wound closure. *Mathematical Biosciences*, 252: 45:49, 2014.

[**5**] B. M. and J. McGrath. Sheet migration by wounded monolayers as an emergent property of a single-cell dynamics. *J. Cell Sci*, 120:876:884, 2007.

[**6**] C. O. G.-M. E. S. P. H. V. Sepúlveda N., Petitjean L. Collective cell motion in an epithelial sheet can be quantitatively described by a stochastic interacting particle model. *PLOS Computational Biology*, 9:3, 2013.

[**7**] G. N. S.-P. M. G.-M. E. Shirley M., Shlomovitz R. and S. P. Physical model of the dynamic instability in an expanding cell culture. *Biophysical Journal*, 98:361:370, 2010.

[**8**] A. T. M. E. W. D.-B. J. Trepat .X, Wasserman M.R. and F. J.J. Physical forces during collective cell migration. *Nature Physics*, 5:426:430, 2009.

[**9**] J. E. Vermolen F.J. Computer simulations from a finite-element model for wound contraction and closure. *Journal of Tissue Viability.*, 19:43:53, 2010.

CHAPTER

FOUR

Electric fields and impedance characterization in cell monolayer

Contents

4.1 Introduction

The migration of healthy cells to the injured site is one of the most important processes during wound healing. Wound healing may be compromised due to a lack of proliferation, but it can also fail due to the inability of cells to migrate into the wound zone. The field of electrophysiology explores the mechanisms of electric signal generation and propagation in living tissues. The maintenance of a potential across the plasma membranes of both nervous and muscle cells has been widely studied [28],[24]]. However, no confirmed evidence of the existence of electric currents in wounds was not confirmed. Similarly to nervous and muscle cells, epithelial cells are able to maintain a potential across the epithelium, called transepithelial potential (TEP), that is the sum of all of the plasma membrane potentials that compose the epithelium that are maintained through the transport of ions. It has been reported that depending on the measured region, the voltage across epithelial cells in humans ranges from 10mV to 60mV [18]. An intact epithelium transports ions inwards and outwards the cell membrane and after the generation of a wound the epithelial barrier is disrupted, and this short-circuits the epithelium and therefore a drop in the potential at the wound occurs [19]. The generation of this potential gradients leads to the production of a current that flows to the more negative site (inside the wound), creating orientated wound electric fields ([23] ,[18]).

External applied electric fields similar in magnitude to the endogenous electric fields (EEFs) induce cell migration. In the case of skin cells such as fibroblasts and keratinocytes, they exhibit cathodal migration in applied electric fields (EFs). This induced migration polarizing cells towards the wound is called galvanotaxis ([31],[22]). As a result of the application of an external electric field in the default healing direction, the migration significantly increases [18]. On the other hand, if the electric field is applied in the anodal direction, i.e. against the natural healing direction, the migration is decreased or even stopped, showing that when an EF is applied, cells are able to ignore any other signals that drive migration, such as chemotaxis, contact inhibition release or population pressure.

After the injury, at the initial stages, epithelial cells may communicate with each other through the fast propagation of [Ca2+] waves helping neighbouring cells to induce migration and proliferate in order to repair the wound [15]. Calcium-sensing receptor (CaSR) is implicated in cell migration and proliferation processes. On the other hand, mechanical injury produces an internal

[Ca2+] wave propagation which suggest a link of CaSR between cell-cell communication and reepithelization during wound healing. Besides, several studies have shown that, in most of the cells, Ca2+ is one of the main ions involved in galvanotaxis [21]. When a direct current electric field (dcEF) is applied to the cells a rise in Ca2+ concentration increases in a given part of the cell, causing its contraction, whereas the other part of the cell will relax by a reduction of calcium concentration. Thus, creating a push-pull movement and therefore, migration.

Epithelial layers control diffusive permeation of solutes along intercellular clefts between adjacent cells and can also actively transport substances along transcellular paths. Cells are connected and sealed at the apical region by tight junctions, which are the key components of epithelial and endothelial cell barriers ([1],[13]). These tight junctions are of special relevance for the active barrier functionality of the cell layer. They regulate the passage of molecules through the barrier, acting as a specialized intercellular junctional complex, as they selectively open and close in response to various signals from the inside and outside of the cells.

The transport of substances across epithelial cells can be either paracellular or transcellular. The paracellular transport of molecules refers to the transfer of substances across the intercellular space between cells, thus, across tight junctions [6]. On the other hand, in transcellular transport, substances travel through the cell, passing both the apical and basolateral membranes [25]. As it has been previously mentioned, electric current flow through epithelial cells is caused by ion flow. Hence, all the transport mechanisms allowing the passage of ions either across or through epithelial cells exhibit a resistance. With the generation of a wound in an epithelial sheet, the electrical impedance created by the paracellular transport structures, tight junctions will be disrupted, and therefore the epithelium will be short-circuited. Thus, causing a drop in the monolayer overall resistance [19].

Nowadays, one of the main methods for measuring monolayer impedance is the commercial device Electric Cell-substrate Impedance Sensing (ECIS). For this technique, cells are directly seeded on the electrode, thus loosing theeffect of the culture media between cells and electrodes since they are in direct contact. This method can be used for real-time monitoring of cell behaviour such as, adherence, mobility and growth on solid substrates [8]. Another posibility are the microfabricated galvanotactic chambers [11]. In the present work, impedance spectroscopy methods will be used in order to monitor and analyse

epithelial monolayers impedance through an Impedance/Gain-Phase Analyzer and a simple self-designed measuring electrode system.

4.2 Materials and methods

4.2.1 Cell culture

HaCaT cells, an immortalized keratinocyte cell line, used for this study were provided from Centro de Investigaciones Energeticas Medioambientales y Tecnologias (CIEMAT) and cultured in DMEM (Gibco Dulbeccos Modified Eagle Medium), supplemented with 10% Fetal Bovine Serum (FBS) and 1% Antibiotic/Antimycotic (Ab/AM) from Thermo Scientific HyClone. Keratinocytes cultures were established following the standard protocols from Arakawa, Y. et al. [12].

To perform experiments, cells were washed with PBS 1X and then detached with Trypsin 1X (Sigma Aldrich) incubating them at 37°C for 10 minutes. Cells are then centrifuged and re-suspended in fresh growth media so they were seeded on p-35 petri dishes at a density of 40000 cells/mm^2, reaching confluence after 24 hours of incubation at 37°C and 5% CO2. This procedure was performed in a laminar flow hood in sterile conditions.

4.2.2 Impedance measurement assay: confluent and wounded monolayer

We performed two sets of experiments, one characterizing the impedance of a confluent epithelial monolayer and another one simulating the process of wound healing. In both cases a voltage difference was applied in order to characterize the frequency response of the impedance. For the performance of both migration and impedance experiments, two handmade devices were designed. They are composed of a p-35 petri dish lid through which two silver alloy wires are introduced and supported by a transparent PDMS piece attached to the lid. This PDMS support allows correct visualization of the migrating monolayer through the microscope while assures the precise position of electrodes. To study how distance affects impedance measurements, two devices were designed by changing the distance between the electrodes, setting it to 6 mm and 30 mm. This allows us to subject cells to different electric fields (mV/mm) applying the same voltage difference.

In migration experiments, monolayers were seeded with a PDMS stencil used as a barrier to avoid cell invasion, following protocols from [29], and restricting cell cultrure just to one half of the dish as illustrated in figure 4.1. Semi-infinite wounds were analysed, considering just one half as a simplification of the problem. The day after seeding, the stencil is carefully peeled off so that cells can migrate to the free space released. This methodology avoids cell damage at the edge compared to simple pipette scratching [26]. PDMS stencils were fabricated in the laboratory and were used in order to cover half of the surface of a p-35 petri dish. To start the experiment, the lid is placed on top of the culture dish so the wires perfectly matched the surface of the cell monolayer and then they were connected to the impedance gain-phase analyser.

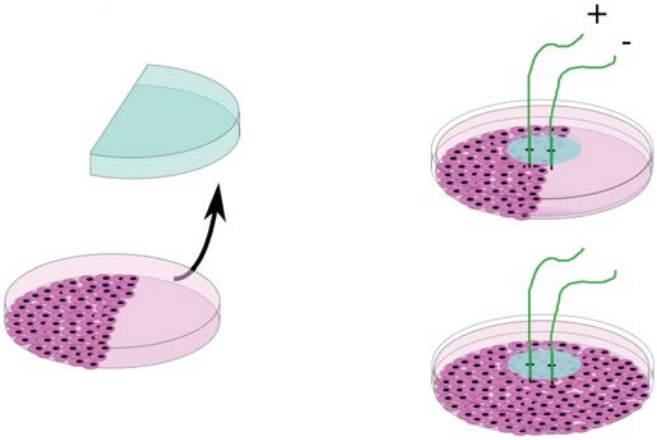

Figure 4.1: Schematic representation of the cell culture set up for confluent and migrating monolayers

To fully characterize the system impedance we divided the frequency spectrum under study into two sets, one at high frequencies (from 10^3 Hz to 10^5 Hz) and then we decided to move to a lower frequency range (from 10^{-1} Hz to 10^2 Hz). Three DC voltage signals were applied at 0, 50 and 100 mV with 20mV of AC in the frequency spectrum from 10 kHz to 0.1 Hz.

To perform time-lapse microscopy during migration experiments cells were maintained in incubation system (OKOLab) which preserves incubation conditions of temperature (37°C), humidity (40%) and CO2-air concentration (5%).

4.2.3 Calcium concentration measurements

Intracellular Ca2+ concentration in wounded HaCaT cells were imaged using cell permeant Fluo-4 AM. Fluo-4 AM Starter Pack (Invitrogen) contains 3 components, Fluo- 4 Direct calcium assay reagent, probenecid water-soluble and Fluo-4 Direct calcium assay buffer. A 250 mM stock solution was prepared by adding and vortex Fluo-4 Direct calcium assay buffer to the water-soluble probenecid. Probenecid was used to inhibit organic-anion transporters located in the cell membrane that can extrude the dye, contributing to poor loading. Finally, a 2X Fluo-4 Direct calcium reagent loading solution composed of Fluo-4 Direct calcium reagent and the stock solution was prepared following protocols from the supplier.

Once the cells have reached confluence the stencil is carefully peeled off and 1 mL of loading solution and 1mL of culture media were added. Finally, they were incubated at 37°C for approximately 45 minutes. Then fluorescence was measured using 494 nm as excitation wavelength and emission at 516 nm.

The fluorescence microscopy used in order to perform the imaging of Fluo-4 AM dye was Olympus CKX-41 inverted microscope equipped with Olympus U-RFL-T mercury burner our imaging purposes FITC filter was used.

4.2.4 Computational analysis

The complex impedance expression is calculated from the frequency response of experimental data provided by the impedance gain-phase analyser. Then, the roots (poles and zeroes) of the characteristic equation of the system are analysed by means of custom-made Matlab programs. Finally, these roots lead to a suitable equivalent system that was designed based on previous published works ([3], [**?**], [14]) that can be compared to experimental data.

Impedance estimation

The experimental data obtained from the gain-phase impedance analyser is the electric response of the cells under certain circumstances such as external electric field or TEP disruption. From the electrical characterization of an epithelium can provide information of morphological changes and can be related to metabolic activities [10]. Besides, this could help to deeply understand biological processes, for instance wound healing, or even more complex problems as cancer or cell mutations.

The experimental data can be fitted to an analytical expression for a transfer function, in our case impedance function, defined by some roots of both the numerator (zeros) and denominator (poles). Depending on the nature of these roots the system may be either stable or unstable [2].

Equivalent-circuit design

The impedance of an AC circuit can be expressed as an impedance function or Z(s). The polynomials in the numerator and denominator are the combination of impedances of both the resistances (Zr = R) and capacitors (Zc = 1/(jwC)) of the circuit, real and imaginary respectively. The experimental impedance obtained in this study is represented by its magnitude and phase, which is the lag existing between current and voltage amplitudes [2]. Since we already know the behaviour of basic electric components (resistances and capacitors) we can design an equivalent circuit that provides the same response to the applied voltage as the experimental data. We could then analyse different experimental conditions, cells, drugs... to compare and better understand the system response.

4.3 Results

4.3.1 Experiments at confluence

One of the main goals of this study is to evaluate the influence that different external voltages may have on the impedance of a cell monolayer and fully characterize its electrical behaviour.

With this purpose, cells were seeded to confluence and stimulated with DC voltages of 0, 50 and 100 mV with an overimposed AC voltage of 20mV. The frequency range was first from 0.1 kHz to 10^5 kHz, in order to reduce acquisition time (figure 4.2).

Figure 4.2 shows the frequency response of the measured impedance on confluent monolayers subjected to different DC voltages applied with two electrodes separated by 6 mm but always with the same AC signal of 20 mV of amplitude.

On panel 4.2(a), the modulus of the impedance is represented. First we can highlight that there are no significant differences on the impedance curves for the three applied voltages, meaning that monolayer impedance exhibit a linear impedance within the range of voltages considered here.

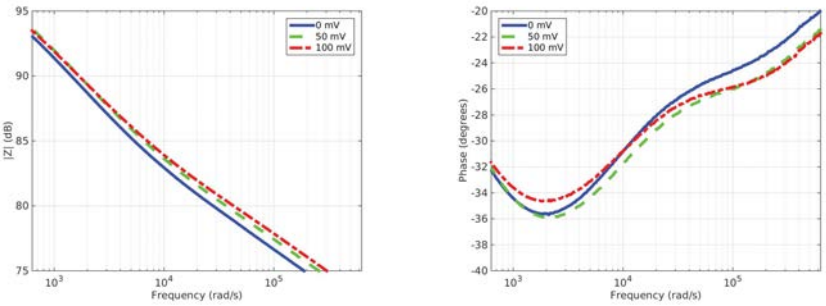

(a) |Z| (dB) vs. Frequency (rad/s) (b) Phase (degrees) vs. Frequency (rad/s)

Figure 4.2: Impedance response at high frequency response range. diagrams show the confluent monolayer behaviour at different external applied voltages. Frequency range: 0.1 - 10^5 Hz. DC voltage 0, 50, 100 mV, AC voltage 20 mV.

Change in slope?

10^3 – 10^4H slope = –10dB/decade
10^4 – 10^5Hz slope = –5dB/decade

The offset between curves is the resistance.

In panel 4.2(b), the phase change of the impedance is shown varying from –20 and –35°. It first shows a decrease until 2000 rad/s where it starts growing as the frequency grows.

Since, in general, the cell mechanical response is slower compared to the applied frequency signals, measurements were repeated for smaller frequency ranges. But regarding that the DC voltage applied had no influence on impedance response for the experiments performed at low frequency (0.1 to 10^3 Hz) just the external voltage of 50 mV was studied keeping the overimposed AC voltage at 20 mV.

Since cells need culture medium to be alive the impedance measurements are a combination of both contributions, the cell monolayer and the culture medium. In order to obtain the cell impedance we performed two types of experiments, the culture medium alone and the cell monolayer covered with medium. Then the culture media impedance is properly subtracted to obtain the impedance characterization of the cell monolayer, as it is shown in figure 4.3(a). In the case of the cells, impedance decays at the rate of -10 dB/decade.

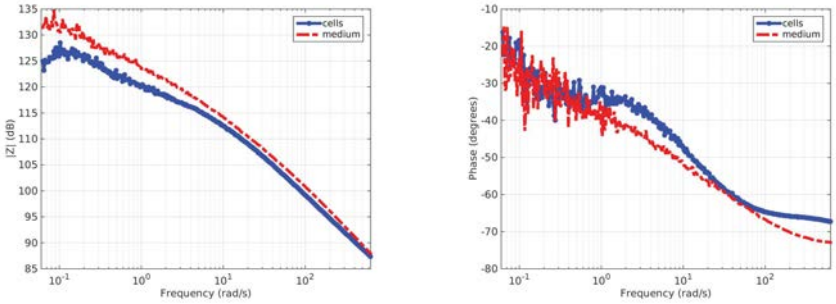

(a) |Z| (Ohms) vs. Frequency (rad/s) (b) Phase (degrees) vs. Frequency (rad/s)

Figure 4.3: Impedance frequency response, diagrams obtained for different voltages on a confluent monolayer. Frequency range 0.1-100 Hz. DC voltage 0, 50, 100 mV, and overimposed AC voltage of 20 mV.

At the frequency of 3-4 rad/s the slope increase slightly to -15 dB/decade. At lower frequencies the phase (figure 4.3(b)) exhibits a noisy behaviour, this resonance could be related to another capacitor at low frequency that implies that we are only measuring the impedance of the culture medium.

In order to propose an equivalent circuit that represent the electric behaviour of the system under study the frequency response of both magnitude and phase of the impedance should be taken into consideration.

4.3.2 Migration experiments

As has been previously mentioned, the impedance of a monolayer is established by both the resistance of the transcellular and paracellular current routes. In the presence of a wound, the overall impedance of the monolayer drops, due to the loss of tight junctions' resistance [18]. Furthermore, once the healing mechanisms are activated, that drop in the impedance should be recovered over time, until reaching its maximum, which corresponds to the value measured in confluence [28].

For this section, several experiments have been performed by generating a wound and analysing both the evolution of the impedance and the cell migration velocity under the effects of DC voltages ((1) 0mV, (2) 50mV, and (3) 100mV) in a frequency range between 0.1Hz and 100Hz (figure 4.4) with a sampling distance between the electrodes of 6 mm.

For all the experiments illustrated in figure 4.4, it can be observed that the

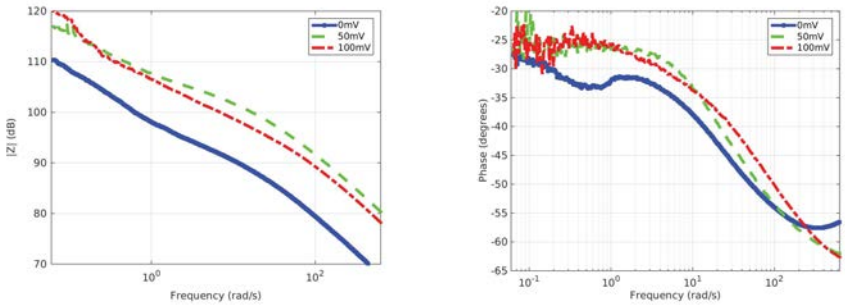

(a) |Z| (dB vs. Freq (rad/s)

(b) Phase (degrees) vs. Frequency (rad/s), Range (0.1-100 Hz)

Figure 4.4: Bode diagrams obtained applying different voltages on a wounded monolayer. Frequency Range (0.1-100 Hz). Migrating cells were stimulated with 0 mV, 50 mV and 100 mV

impedance is lower than the one measured in confluence (one order of magnitude), coinciding with the previous stated theory [9]. However, the experiment duration has not been enough for the monolayer to cover the whole wound (nor the two electrodes) and therefore, the values have not reached those of confluence. However, it can be observed that with time(figure 4.5(a)) the impedance was rising, approaching those of confluence. Figure 4.4(a) shows the same behaviour as that observed in the previous ones (figures 4.2 and 4.3), namely that the greater values of impedance are found at the smaller frequencies. The difference in impedance (figure 4.4(a)) that is created by the stimulation of cells with voltage can only be noticed at low frequencies as it happened in confluent experiments, showing that the higher the voltage applied, the greater the impedance.

On the contrary, the phase is quite the same in the three cases, same behaviour no matter the voltage applied. Since, every cell is subjected to higher voltage, the resistance they oppose to the electric current to flow, is higher

These changes can be related to migration velocity induced by the electric fields (figure 4.5(b)). An increase in healing velocity means that cells will reach confluence faster, and therefore the impedance of a healthy monolayer will be reached.

Figure 4.5(a) reveals that the experiments exposed to electric fields show a faster impedance growth approaching to confluent values and figure 4.6 exhibit

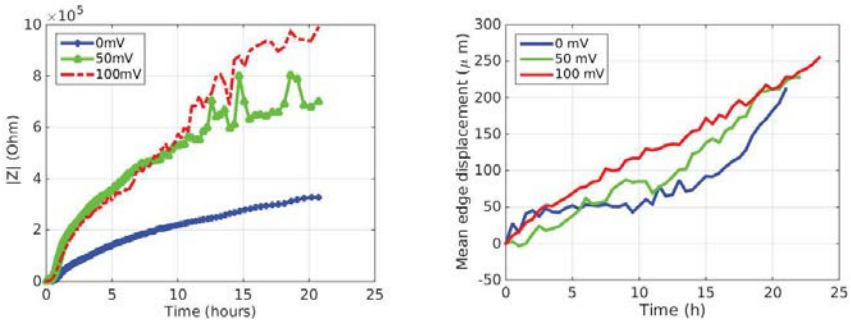

(a) Evolution of the impedance with time

(b) Mean edge displacement with time

Figure 4.5: Temporal evolution of measured impedance and meand edge displacement of different monolayers stimulated with 0mV,50mV and 100mV

that the disruption of the cellular confluency implies a drop in the impedance.

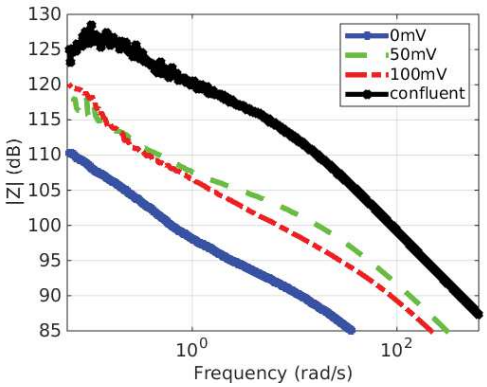

Figure 4.6: Impedance response of migrating monolayers excited with different voltages and confluent monolayer

The plot on 4.7 shows the impedance complex response for three migration experiments stimulated with and external electric field of 0, 50 and 100 mV and an effective distance between the electrodes of 6 mm.

Semicircles within the high frequency window display the charging of double layers on the system within the electrode and the contribution of different resistances. At lower frequencies, a "tail" is shown. The shape of the tail is principally affected by the diffusion within the electrolyte and the active electrode material (cell monolayer in our case). The real impedance at the leftmost point

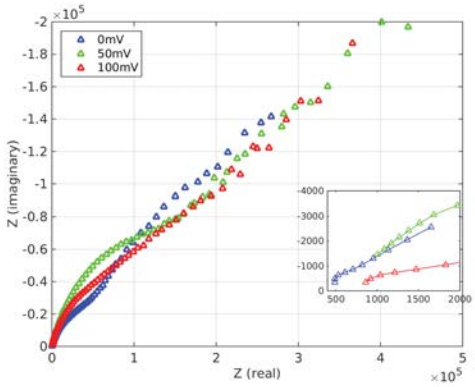

Figure 4.7: Impedance complex plane plot for three different migration cases

in the Nyquist plot gives the measure of the ionic and electrical conductivity within the system.

4.3.3 Equivalent circuit modelling

Z(s) estimation on confluent monolayer

Once the effects that voltage has on an epithelial monolayer have been studied, an equivalent circuit representing the monolayer will be proposed. To do so, first of all an analytical expression of the frequency response of the impedance is computed from the experimental data obtained though curve fitting module from Matlab. The impedance function can be estimated by searching the best possible fit varying the possible number of zeros and poles. We have considered that the medium impedance is in parallel with the cell monolayer impedance. Since we have the frequency response of both, the media (Z_m) and the media with the cells (Z_{mc}) we can subtract the impedance of the cells (Z_c):

$$Z_c = \frac{Z_{mc} \cdot Zm}{Zm - Zc} \tag{4.1}$$

After exploring different configurations, the best pole-zero combination found is 2 poles and 2 zeros reaching an estimation fit between 77 % (4.8), considering the inherent variability that exists in the experimental setup this result is quite accurate.

$$Z_{fit} = \frac{4.2 \cdot 10^3 s^2 + 1.45 \cdot 10^7 s + 4.95 \cdot 10^6}{3.7 s^2 + 9.03 s + 1} \ (\Omega) \tag{4.2}$$

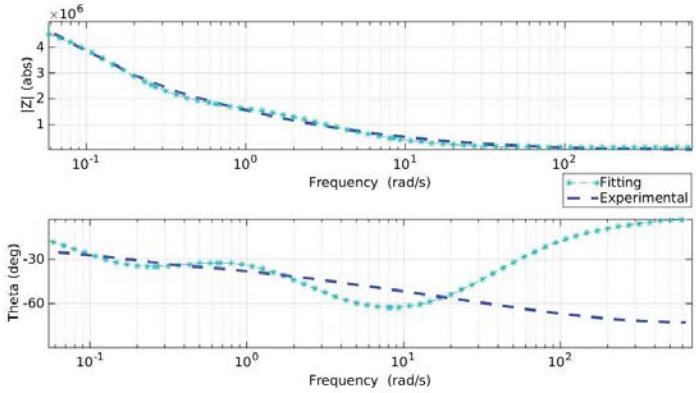

Figure 4.8: Fitting cell impedance assuming parallel configuration between the monolayer and medium.

Although the module of the impedance is estimated quite well,the phase-response is not well captured by the fitting function. Actually, two poles and two zeroes introduce high variation in phase at higher frequencies as it can be appreciated in figure 4.8.

Equivalent-circuit design

After obtaining the estimated impedance function, one can proceed to the design of an equivalent electric circuit whose behaviour is also represented by the impedance function. Both expressions, the analytical presented in equation 4.3 and the experimental one from the fitting (equation 4.2) can be compared. The proposed equivalent circuit (figure refcircuit) has been inspired in previous ones designed by other research groups ([8], [7]).

The 4.9 represents two sample cells contained in an epithelial monolayer. To model the circuit, it has been taken into account both the resistance of the intracellular transport (R2,C2,R3) driven by the impedance that the cell has itself, along with that of the transcellular one(R1,C1) result of cell-cell communication .

The expression for the impedance of the cell monolayer follows:

$$Z_{cell} = \frac{R_1R_2R_3C_1C_2\,(j\omega)^2 + ((R_2+R_3)\,R_1C_1 + R_2R_3C_2)\,j\omega + (R_2+R_3)}{(R_2R_3C_1C_2 + R_1R_2C_1C_2)\,(j\omega)^2 + ((R_2+R_3)\,C_1 + R_1C_1 + R_2C_2)\,j\omega + 1} \tag{4.3}$$

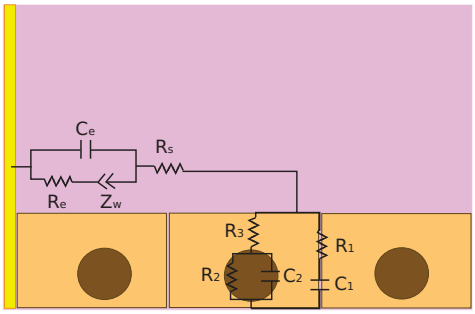

Figure 4.9: Circuit representing the epithelial monolayer in parallel with the culture medium

To model the culture media, we chose a Warburg impedance element. Warburg impedance is caused by the diffusion of ions from bulk electrolyte solution to the electrode-electrolyte interface [17].

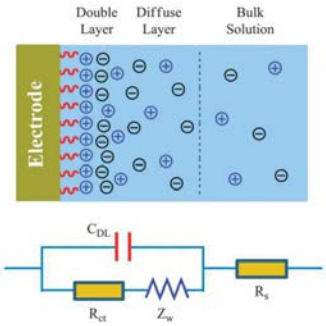

Figure 4.10: Electrode-electrolyte interface modelled with a Warburg element that reproduces the diffusion of ions from the electrode to the bulk solution

Re: electrolyte resistance Ce: capacitance of the electrode Zw: diffusion of ions

$$Z_\omega = \sigma\sqrt{\omega}(1-j) \tag{4.4}$$

Taking into consideration theses elements the expression for the culture media impedance

$$Z_{media} = \frac{j\omega^3 C_e R_e + R_e + \sigma\sqrt{\omega}(1-j)}{j\omega^3 C_e + 1 + Rs} \tag{4.5}$$

We obtained a 79 % fitting of the theoretical expression of the Warburg equivalent circuit (equation 4.5) to the experimental data.

Comparing the analytical expression of the impedance obtained from the equivalent circuit and the numerical fitting of the experimental data, we can quantify the values of the theoretical components of the proposed circuit that are shown in table 4.1.

R_1	0.105 MΩ
R_2	6.03 MΩ
R_3	2.32 kΩ
C_1	1.61 mF
C_2	21.7 μF

Table 4.1: Table of fitted values from experimental data

Considering that the external voltage that is applied in the confluent monolayer is divided among all the cells found between the electrodes, each cell is subjected to:

$$V_i = \frac{I_i i}{j\omega C_i} \tag{4.6}$$

$$V_{eq} = V_1 + V_2 + ...V_i + ...V_N = \frac{I_1}{j\omega C_1} + \frac{I_2}{j\omega C_2} + ... + ..\frac{I_i}{j\omega C_i} + ...\frac{I_N}{j\omega C_N} \tag{4.7}$$

Since connected components in serial (in this case, confluent cells) have identical current:

$$V_{eq} = \frac{I}{j\omega} * \left(\frac{1}{C_1} + \frac{1}{C_2} + ... + \frac{1}{C_i} + ... + \frac{1}{C_N} \right) = \frac{I}{j\omega} * \frac{1}{C_{eq}} \tag{4.8}$$

Assuming all cells have the same capacitance (C):

$$V_{eq} = \frac{I}{j\omega} * \frac{N}{C} \tag{4.9}$$

Being N the number of cells between the electrodes, the bigger the sampling distance, the higher N becomes, thus leading to a greater value of the impedance. In the case of the disrupted monolayer, current will flow through the cells (transcellular connection) but, since the number of cells between the

electrodes has decreased, the voltage is distributed partly among the cells and partly within the culture media, which is more conductive due to its electrolytic nature. This is going to produce a decrease in its impedance. This is the behaviour observed in migrating monolayers, a drop in the impedance compared to the measurements at confluence.

With this idea we propose that the system has the following equivalent circuit representing its behaviour (figure 4.11):

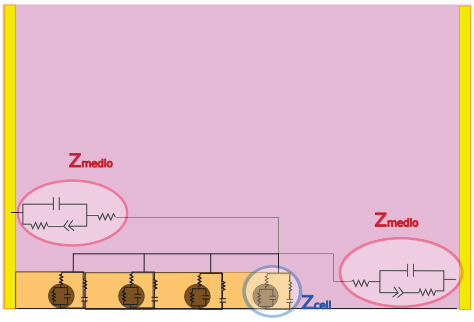

Figure 4.11: Schematic representation of the equivalent circuit of a migrating monolayer

In figure 4.11 we propose a model where the disrupted monolayer is in parallel and in serial connection to the culture media leading to the following expression, regarding that our measurements are in one hand the culture media itself (Z_m) and on the other hand, the monolayer with the culture media(Z_{mc}). So, to isolate the monolayer impedance alone (Z_c), we have considered this configuration leading to:

$$Z_c = \frac{Z_m(Z_m - Z_{mc})}{Z_{mc} - 2Z_m} \tag{4.10}$$

From the experimental data, we can operate with the impedance measurement of both Z_{mc} and Z_m that could provide us the disrupted monolayer impedance for further analyses.

4.3.4 [Ca2+] measurements in wounded monolayer

One of the main ions driving cell migration is Ca2+ ([27], [16]), so in order to determine whether a traumatic stimulus like the one studied here generates a Ca2+ response, calcium concentration in wounded monolayers were

stained with Fluo4-AM (Sigma Aldrich). Moreover, in previous publications ([18],[11],[5]) it has been proven that voltage influences migration, and therefore, stimulation with different magnitudes of voltage should also elicit a calcium response (figure 4.12).

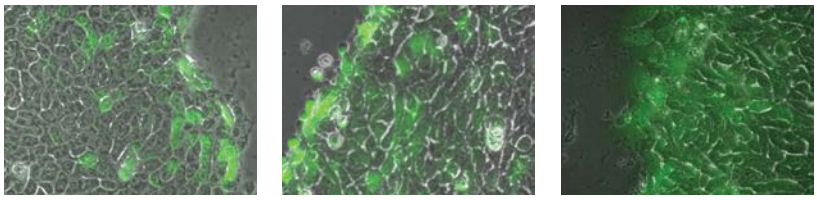

(a) Calcium imaging 0mV at t=0h (b) Calcium imaging 50 mV at t=0h (c) Calcium imaging 100 mV at t=0h

Figure 4.12: Imaging of intracellular calcium at the monolayer edge labeled with Fluo4AM rigth after the wound creation and the application of the three different voltages under study

Fluo4 dye shows intracellular calcium ions in green colour in fluorescence microscopy, increasing intensity with an increase in calcium ions inside the cell. As shown in 4.12, at 0 hours, Ca2+ concentration increases at the wound edge, and this elevation is spread to the neighbouring cells. In the samples affected by voltage a higher concentration of Ca2+ is observed, increasing as voltage is increased, and affecting a higher number of surrounding cells. Furthermore, the cells were incubated 24 hours and their calcium response was also analysed (4.13). In this case, it can be observed that throughout 24h the calcium response has been transmitted many rows in the remaining monolayer for all the experiments. However, differences on intensity given by the calcium dye can be still perceived between the cells subjected to voltage and those that are not. At this point, all the monolayers are at its maximum velocities, causing this extended Ca2+ response and showing no significant difference among them.

24h after wounding the monolayer, the collective migration is already stablished and the intracellular Ca2+ is homogeneously spread in the three cases with no remarkable differences (4.13).

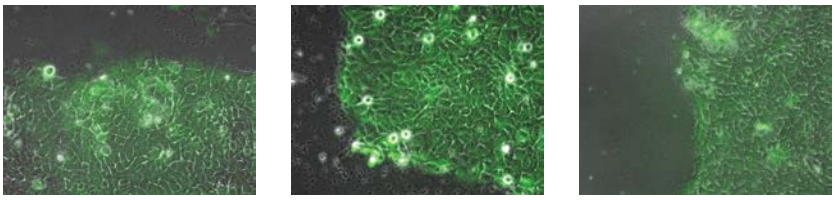

(a) Calcium imaging 0mV at t=24h

(b) Calcium imaging 50 mV at t=24h

(c) Calcium imaging 100 mV at t=24h

Figure 4.13: Imaging of intracellular calcium at the monolayer edge labeled with Fluo4AM 24 hours after the wound creation and the application of the three different voltages under study

4.4 Discussion

In the present work electrical characterization of an epithelial monolayer in both confluence and migration states have been performed serving to deepen the understanding of the mechanisms taking place during migration in the wound healing process.

First, measurements at high frequencies showed less influence by the sampling area with respect to those at lower frequencies, that detect higher impedance when measuring a smaller sampling area, as it was proven by Ahmed et al. [4], when they measured the influence of electrode geometry on impedance spectroscopy.

The impedance response in confluent monolayers were numerically fitted leading to a 2-pole and 2-zero impedance function (around 80 % of fitting). On the other hand, based on previous works, we proposed an equivalent circuit that mimics the confluent monolayer electrical behaviour and provided a theoretical expression of the impedance. Then, both results the experimental and theoretical, were compared providing the exact values for those electrical components inside the cells. This result allowed us to study the influence the electric field has, suggesting a direct implication on cell-cell communication.

Moreover, the impedance response was measured during monolayer migration showing how these values during migration progressively approached to confluence values as the monolayer tend to cover both electrodes. The results have confirmed that, indeed, as the wound edge migrates towards closure, the measured values increase to attain confluence values, as it had been previously stated by Wegener et al. [30]. Furthermore, this increase on the impedance has

been related to the effects that induced external electric fields have on migration. In previous studies such as the one acomplished by [20] and [18], it was demonstrated that when a wounded monolayer is applied with low intensity voltages, the leading edge migration velocity increases. Here, it has been shown that an increase in migration velocity due to externally induced electric fields triggers an increase in the rate at which impedance values reach its maximum ones.

Additionally, for a further comprehension of how the factors involved in migration are affected by induced electric fields, intracellular calcium was stained in order to observe how applied voltage impacts its concentration on the wounded cells. It has been observed that, right after the generation of a wound in a monolayer, the number of cell rows behind the edge with intracellular calcium concentration marked with Fluo4AM increases with the voltage applied. Moreover, 24 hours after the generation of the wound, the calcium response was extended many rows behind the leading edge, coinciding with the time at which the migration velocity is maximum; although no difference in calcium concentration between applied voltages was observed.

Nomenclature

TEP	Transepithelial potential
EEF	Endogeneous Electric Field
EF	Electric Field
CaSR	Calcium Sensing Receptor
dcEF	direct current Electric Field
ECIS	Electric Cell-substrate Impedance Sensing
CIEMAT	Centro de Investigaciones Energeticas Medioambientales y Tecnologicas
Ab/AM	Amtibiotic Antimicotic
DMEM	Dulbeco's Modified Eagle Medium
PBS	Phosphate Buffer Serum
PDMS	Polydimethylsiloxane
DC	Direct Current
AC	Alternating Current
FITC	Fluorescein isothiocyanate
AC	Alternating Current

Bibliography

[**1**] *Essential cell biology(2nd ed.)*. Garland Science, 2004.

[**2**] *Fundamentals of Electric Circuits*. âĂć, 2009.

[**3**] *Handbook of bioelectronics. Directly interfacing electronics and biological systems*, chapter Cell array biosensors. Cambrigde University Press, 2015.

[**4**] R. Ahmed and K. Reifsnider. Study of influence of electrode geometry on impedance spectroscopy. *Int. J. Electrochem. Sci*, 2011.

[**5**] e. a. Aihua Guo 1. Effects of physiological electric fields on migration of human dermal fibroblasts. *Journal of Investigative Dermatology*, 2010.

[**6**] J. M. Anderson. Molecular structure of tight junctions and their role in epithelial transport. *News Physiology Science*, 2001.

[**7**] J. M. Anderson and C. M. Van Itallie. Physiology and function of the tight junction. *Spring Harb. Perspect. Biol.*, 2009.

[**8**] C. S. . G. H.-J. Benson, K. Impedance-based cell monitoring: barrier properties and beyond. *Fluids Barriers*, 2013.

[**9**] S. R. W. Charles R. Keese, Joachim Wegener and I. Giaever. Electrical wound-healing assay for cells in vitro. *Procceedings of the National Academy of Science*, 2004.

[**10**] C. R. Chun-Min Lo and I. Giaever. Impedance analysis of mdck cells measured by electic-cell-substrate impedance sensing. *Biophysical Journal*, 1995.

[**11**] W. J. N. Daniel J. Cohen and M. M. Maharbiz. Galvanotactic control of collective cell migration in epithelial monolayers. *Nature Materials*, 13: 409–417, March 2014.

[**12**] Y. A. et. al. Biomedical research. *Low concentration fluoride stimulates cell motility of epithelial cells in vitro*, 30:271:277, 2009.

[**13**] J. Fromter, E. & Diamond. Route of passive ion permeation in epithelia. *Nature: New Biology*, 1972.

[**14**] O. A. S. Isaac O. KOwino. Impedance spectroscopy: A powerful tool for rapid biomolecular screening and cell culture monitoring. *Review in Electroanalysis.*, 2005.

[**15**] A. S. T. P. E. J. M. J. C. Javier Milara, Manuel Mata. Extracellular calcium-sensing receptor mediates human bronchial epithelial wound repair . *Biochemical Pharmacology*, 2010.

[**16**] A. B. Lansdown. Calcium: a potential central regulator in wound healing. *Wound Repair and Regeneration*, 2002.

[**17**] X. Luo and J. J. Davis. Electrical biosensors and the label free detection of protein disease biomarkers. *Chemical Society Review*, 2013.

[**18**] Z. M. Electrical fields in wound healing-an overriding signal that directs cell migration. *Seminars in Cell and Developmental Biology*, 2009.

[**19**] R. A. M. S. B. . Z. M. McCaig, C. D. Controlling cell behavior electrically:current views and future potential. *Physiology Review*, 2005.

[**20**] J. P. T. W. B. R. G. T. F. W. A. G. P. W. . Y. G. . T. S. . A. S. . J. V. F. . H. R. B. P. N. D. C. D. M. Min Zhao, Bing Song and J. M. Penninger. Electrical signals control wound healing through phosphatidylinositol-3-oh kinase-γ and pten. *Nature Letters*, 442:457–460, July 2006.

[**21**] M. B. a. Mycielska, M. E. & Djamgoz. Cellular mechanisms of direct-current electric field effects: galvanotaxis and metastatic disease. *Journal of Cell Science*, 2004.

[**22**] I. R. R. . N. R. Nishimura, K. Y. Human keratinocytes migrate to thenegative pole in direct current electric fields comparable to those measured in mammalian wounds. *Journal of Cell Science*, 1996.

[**23**] R. Nuccitelli. Endogenous ionic currents and dc electric fields in multicellular animaltissues. *Bioelectromagnetics*, 1992.

[**24**] K. R.D. and A. D.J. Nerve and muscle. 2nd edition. *Journal of the Marine Biological Association of the United Kingdom*, 72(2):509âĂŞ509, 1991. doi: 10.1017/S0025315400037929.

[**25**] L. Reuss. Epithelial transport. *Handbook of Physiology*, 1997.

[**26**] D. D. Z. P. K. W. Reza Riahi*, Yongliang Yang*. Advances in wound-healing assays for probing collective cell migration. *Journal of Laboratory Automation.*, 2012.

[**27**] A. Schwab. Function and spatial distribution of ion channels and transporters in cell migration. *Americal Journal of Physiological Society*, 2001.

[**28**] S. Thesleff. Nerve and muscle excitation, second edition. *Muscle & Nerve*, 4(6):533–533, 1981. ISSN 1097-4598. doi: 10.1002/mus.880040616. URL http://dx.doi.org/10.1002/mus.880040616.

[**29**] L. C. Vedula E.R.K., Ravasio A. and L. B. Collective migration: a mechanistic perspective. *Physiology*, 28:370:379, 2013.

[**30**] K. C. R. Wegener, J. and I. Giaever. Electric cellâĂŞsubstrate impedance sensing (ecis) as a noninvasive means to monitor the kinetics of cell spreading to artificial surfaces. *Experimental Cell Research*, 2000.

[**31**] X. L. J. Q. C. T. Yu Wang, Guixue Wang. Substrate stiffness regulates the proliferation, migration, and differentiation of epidermal cells. *Burns*, 38:414:420, 2012.

CHAPTER

FIVE

General conclusions

Contents

5.1 Conclusions

A brief summary of the main conclusions obtained during this dissertation is exhibit during this chapter, although they have been discussed in detail at the end of each chapter.

Epithelial migration is present in many biological processes such as immune response, cancer invasion, immune response or wound healing Understanding the process from a mechanical or physical point of view is a relatively new discipline.

The spatiotemporal distribution of velocity within the epithelium has been studied in cellular monolayers smaller than our system. We introduce the novelty of cells' centroid detection in phase contrast image by means of image segmentation algorithm. This technique allowed us to characterize density distribution in time and space.

To understand the role of proliferation governing this processes we performed experiments in normal conditions and in starvation, inhibiting the ability of cells to proliferation without compromising cell viability.

Velocity fields have shown very different profiles in the two case studies. Experiments performed in starvation showed an initial intent of coordination exhibiting an increase in velocity although it rapidly decayed and some time later finally stopped. On the other hand, those experiments performed at normal conditions showed a long lasting behaviour of coordination within the monolayer. Nevertheless both agreed in slightly smaller velocities in those cells found many rows behind the border, thus spotting fastest cells at the leading edge.

On the contrary, the analysis of the density in both cases have drawn to fascinating and unexpected results. We limited the ability of cells to reproduce in order to force different density distributions but, whereas they end up with the same profiles. This work means a new insight on the relation between cell density and velocity in migration regarding cell proliferation with similar conclusions shown in the work presented by Tlili et al.

To our knowledge just few studies focused on studying the role of density during monolayer migration. Density is a key variable to consider and control in *in vitro* wound healing assays. There is a critical density or threshold below which the coordinated movement to close the wound gap is not established.

Some studies such the ones performed by Tlili et al. and Tremel et al. have proposed and shown that cells far from the edge, since they developed little movement, they provide the tissue with new cells allowing those at the front to keep advancing without breaking the tissue. In the case of starvation, since there is not proliferation cells at some point stop to avoid holes formation or tissue damage.

We performed BrdU staining in order to test where the proliferation is taking place. We were not able to determine the spatio-temporal distribution of cell division with this tool. We could only test that the starvation experiments showed less amount of dividing cells without increasing the apoptotic ones.

Since the stress has to be propagated from the cells found at the edge to the inner tissue to coordinate the movement towards the free space, we also stainned the F-actin fibers to see their the distribution within the monolayer. Although it seemed to be a characteristic length of elongated fibers we were not able to determine it with certain reliability nor define differences between normal conditions and starvation. Nevertheless monolayers subjeted to starvation appeared to be more stretched and stressed. According to Zahm et al. cells cannot do both activities at the same time, if they are involved in a highly coordinated movement trying to close a wound or discontinuity they are not able to reproduce. This phenomenon is commonly known as "go-or-grow" since the cytoskeleton is needed and involved in both processes, cell division and crawling.

In chapter 2 we proposed a in silico model based on precious published work from Banerjee et al. Since in our experiments we were able to measure density we introduced it in the continuum model in order to improve the prediction and results from this kind of models. As a simplification, we decided to start without proliferation since BrdU did not provide us any spatio-temporal distribution of

cell division within the tissue. Besides, we set the polarization force term as a density gradient stablishing that the discontinuity in the monolayer is main driving component of the migration. We fit the termporal evolution of the length of the monolayer as a tool to achieve the value of the free parameters from the model. With the resulting parameters we obtained the rest of the variables conforming the model, de displacements, density and concentration of contractile units.

We found that the initial size of the tissue plays an key role in the model and suggested us that this mathematical models are mainly designed for small systems. Finally we analysed the role the parameters, and besides the terms that go with them, have on the model resulting that diffusivity and internal pressure could be neglected.

In the third chapter we characterize the impedance of a confluent monolayer and then we applied different electric fields on semi-infinite monolayer forcing different kinematic responses. Regarding the impedance data obtained from the phase-gain impedance analyser, we then proposed an equivalent circuit that modelled the transcellular and paracellular communication of the cells. Firstly, we measured the culture media to take into account its impedance due to its electrolitic nature. Then, we measured both together, cells monolayer immersed in culture medium so we could extract medium component from the system and isolate cell monolayer behaviour, With the obtained data we proposed an equivalent circuit that fitted at 80% the experimental data. This model provided the approximate values composing the circuit and gave us some ideas of how cell-cell communication behaves.

Additionally, for a further comprehension of how the factors involved in migration are affected by induced electric fields and we observed that the higher the electric field the largest migration rates the monolayer exhibited. Besides, to deeper understanding of cell-cell communication, intracellular calcium was stained in order to observe how applied voltage impacts its concentration on the wounded cells. It has been observed that, right after the generation of a wound in a monolayer, the number of cell rows behind the edge with intracellular calcium concentration marked with Fluo4AM increases with the voltage applied. Moreover, 24 hours after the generation of the wound, the calcium response was extended many rows behind the leading edge, coinciding with the time at which the migration velocity is maximum; although no difference in calcium concentration between applied voltages was observed.

Alphabetical list of references

[**1**] *Essential cell biology(2nd ed.)*. Garland Science, 2004.

[**2**] *Fundamentals of Electric Circuits*. âĂć, 2009.

[**3**] *Junqueira's basic histology: Text and atlas (Thirteenth edition.)*. âĂć, 2013.

[**4**] *Handbook of bioelectronics. Directly interfacing electronics and biological systems*, chapter Cell array biosensors. Cambrigde University Press, 2015.

[**5**] R. Ahmed and K. Reifsnider. Study of influence of electrode geometry on impedance spectroscopy. *Int. J. Electrochem. Sci*, 2011.

[**6**] e. a. Aihua Guo 1. Effects of physiological electric fields on migration of human dermal fibroblasts. *Journal of Investigative Dermatology*, 2010.

[**7**] J. M. Anderson. Molecular structure of tight junctions and their role in epithelial transport. *News Physiology Science*, 2001.

[**8**] J. M. Anderson and C. M. Van Itallie. Physiology and function of the tight junction. *Spring Harb. Perspect. Biol.*, 2009.

[**9**] S. S. P. V. T. S. Anne Stamm, Kerstin Reimers and I. Pepelanova. In vitro wound healing assays - state of the art. *BioNanoMaterials*, 2016.

[**10**] B. M. H. D. Arciero J.A., Mi Q. and S. D. Continuum model of collective cell migration in wound healing and colony expansion. *Biophysical Journal*, 100:535:543, 2011.

[**11**] R. A. C. W. S. at San Diego State University. Marker-Controlled Watershed Segmentation. URL www.rohan.sdsu.edu.

[**12**] S. Banerjee, K. J. C. Utuje, and M. C. Marchetti. Propagating stress waves during epithelial expansion. *Phys. Rev. Lett.*, 114:228101, Jun 2015. doi: 10.1103/PhysRevLett.114.228101. URL https://link.aps.org/doi/10.1103/PhysRevLett.114.228101.

[**13**] C. S. . G. H.-J. Benson, K. Impedance-based cell monitoring: barrier properties and beyond. *Fluids Barriers*, 2013.

[**14**] L. K. Cai, A.Q. and H. B.D. Multi-scale modeling of awound-healing cell migration assay. *Journal of Theoretical Biology*, 245:576:594, 2007.

[**15**] S. R. W. Charles R. Keese, Joachim Wegener and I. Giaever. Electrical wound-healing assay for cells in vitro. *Procceedings of the National Academy of Science*, 2004.

[**16**] C. R. Chun-Min Lo and I. Giaever. Impedance analysis of mdck cells measured by electic-cell-substrate impedance sensing. *Biophysical Journal*, 1995.

[**17**] W. J. N. Daniel J. Cohen and M. M. Maharbiz. Galvanotactic control of collective cell migration in epithelial monolayers. *Nature Materials*, 13: 409–417, March 2014.

[**18**] T. E. A. K. R. C. Y. P. . X. S.-P. E. H. Z. M. H. Z. J. P. B. D. A. W. J. J. F. Dhananjay T. Tambe, C. Corey Hardin and X. Trepat. Collective cell guidance by cooperative intercellular forces. *Nature Materials*, 10:469–475, June 2011. doi: DOI:10.1038/NMAT3025.

[**19**] Y. A. et. al. Biomedical research. *Low concentration fluoride stimulates cell motility of epithelial cells in vitro*, 30:271:277, 2009.

[**20**] J. Fromter, E. & Diamond. Route of passive ion permeation in epithelia. *Nature: New Biology*, 1972.

[**21**] Y. B. Geoffrey C. Gurtner, Sabine Werner and M. T. Longaker. Wound repair and regeneration. *Nature*, 2008.

[**22**] S. Guo and L. A. DiPietro. Factors affecting wound healing. *Journal of Dental Research*, 89:219–229, 2010.

[**23**] M. G. Habbal A., Barelli H. Assessing the ability of the 2d fisher-kpp equation to model cell-sheet wound closure. *Mathematical Biosciences*, 252:45:49, 2014.

[**24**] K. P. W. H.P.Ng, S.H.Ong. Medical image segmentation using k-means clustering and improved watershed algorithm. *IEEE*, page 61:65, 2006.

[**25**] N. C. Y. H. R. A. G. N. A. S. S. B. P.-L. K. R. R. I. Irena Pastar, Olivera Stojadinovic and M. Tomic-Canic. Epithelilization in wound healing: A comprehensive review. *Advances in Wound Care*, 2014.

[**26**] O. A. S. Isaac O. KOwino. Impedance spectroscopy: A powerful tool for rapid biomolecular screening and cell culture monitoring. *Review in Electroanalysis.*, 2005.

[**27**] B. J. and B. P. Skin structure and function. *Aromadermatology*, 2006.

[**28**] A. S. T. P. E. J. M. J. C. Javier Milara, Manuel Mata. Extracellular calcium-sensing receptor mediates human bronchial epithelial wound repair . *Biochemical Pharmacology*, 2010.

[**29**] A.-L. H. F. D. D. P. P. S. a. E. P. Jean-Marie Zahm, Herve Kaplan. Cell migration and proliferation during the in vitro wound repair of the respiratorio epithelium. *Cell motility and citoskeleton*, 1997.

[**30**] B. A.-L. J. R.-R. A. A. R. A. F. Juan C. del Alamo, Ruedi Meili and J. C. Lasheras. Spatio-temporal analysis of eukaryotic cell motility by improved force cytometry. *PNAS*, 33:13343âĂŞ13348, August 2007.

[**31**] A. J. Kabla. Collective cell migration: leadership, invasion and segregation. *R. Soc. Interface*, 2012.

[**32**] K. Y. S. J. Khammanit R., Chantakru S. Effect of serum starvation and chemical inhibitors on cell cycle synchronization of canine dermal fibroblasts. *Theriogenology*, 70:27:34, 2008.

[**33**] A. B. Lansdown. Calcium: a potential central regulator in wound healing. *Wound Repair and Regeneration*, 2002.

[**34**] L. H. Leeni Koivisto and H. Larjava. Re-epithelialization of wounds. *Endodontic Topics*, 2012.

[**35**] X. Luo and J. J. Davis. Electrical biosensors and the label free detection of protein disease biomarkers. *Chemical Society Review*, 2013.

[**36**] B. M. and J. McGrath. Sheet migration by wounded monolayers as an emergent property of a single-cell dynamics. *J. Cell Sci*, 120:876:884, 2007.

[**37**] Z. M. Electrical fields in wound healing-an overriding signal that directs cell migration. *Seminars in Cell and Developmental Biology*, 2009.

[**38**] A. H. J. J. P. C.-B. L. A. M. Poujade, E. Grasland-Mongrain and P.Silberzan. Collective migration of an epithelial monolayer in response to a model wound. *PNAS*, 104:15988–15993, 2007.

[**39**] O. C.-E. B. L. A. B. S. C. F. A. J. C. M. Reffay, M. C. Parrini and P. Silberzan. Interplay of rhoa and mechanical forces in collective cell migration driven by leader cells. *Nature Cell Biology*, 16:217–223, February 2014.

[**40**] R. Mayor and S. Etienne-Manneville. The front and rear of collective cell migration. *Nature Reviews, Molecular Cell Biology*, 2016.

[**41**] R. A. M. S.-B. . Z. M. McCaig, C. D. Controlling cell behavior electrically:current views and future potential. *Physiology Review*, 2005.

[**42**] D. M. Messerli, M. A. & Graham. Extracellular electrical fields direct wound healing and regeneration. *Biology Bulletin*, 2011.

[**43**] J. P. T. W. B. R. G. T. F. W. A. G. P. W. . Y. G. . T. S. . A. S. . J. V. F. . H. R. B. P. N. D. C. D. M. Min Zhao, Bing Song and J. M. Penninger. Electrical signals control wound healing through phosphatidylinositol-3-oh kinase-γ and pten. *Nature Letters*, 442:457–460, July 2006.

[**44**] P. P. D. MOHAMMAD AMIN and H. BADKOOBEHI. A complete electrical equivalent circuit model for biological cell. In *Selected Papers from the WSEAS Conferences in Hangzhou*.

[**45**] M. B. a. Mycielska, M. E. & Djamgoz. Cellular mechanisms of direct-current electric field effects: galvanotaxis and metastatic disease. *Journal of Cell Science*, 2004.

[**46**] I. R. R. . N. R. Nishimura, K. Y. Human keratinocytes migrate to thenegative pole in direct current electric fields comparable to those measured in mammalian wounds. *Journal of Cell Science*, 1996.

[**47**] R. Nuccitelli. Endogenous ionic currents and dc electric fields in multicellular animaltissues. *Bioelectromagnetics*, 1992.

[**48**] R. P. and M. D.S. Cell density determines epithelial migration in culture. *Proc. Natl. Acad. Sci.*, 77:4760–4763, 1980.

[**49**] J. R. Pierre Recho and P. Marcq. One dimensional collective migration of a proliferating cell monolayer. *soft Matter, Royal Society of Chemistry*, 2016.

[**50**] K. R.D. and A. D.J. Nerve and muscle. 2nd edition. *Journal of the Marine Biological Association of the United Kingdom*, 72(2):509âĂŞ509, 1991. doi: 10.1017/S0025315400037929.

[**51**] L. Reuss. Epithelial transport. *Handbook of Physiology*, 1997.

[**52**] D. D. Z. P. K. W. Reza Riahi*, Yongliang Yang*. Advances in wound-healing assays for probing collective cell migration. *Journal of Laboratory Automation.*, 2012.

[**53**] M. D. Richard A. F. Clark. Cutaneous tissue repair. basic biologic considerations. *Journal of the American Academy of Dermatology*, 1985.

[**54**] P. Roth. Collective cell migration. *Annual Review of Cell and Developmental Biology*, 25:407:429, 2009.

[**55**] J. C. d. A. R. A. F. Ruedi Meili, Baldomero Alonso-Latorre and J. C. Lasheras. Myosin ii is essential for the spatiotemporal organization of traction forces during cell motility. *Molecular Biology of the Cell*, 21:405–417, February 2010.

[**56**] B. L. O. C. B. L. H. D.-A. F. G. S. Tlili, E. Gauquelin. Waves in cell monolayer without proliferation: density determines cell velocity and wave celerity.

[**57**] A. Schwab. Function and spatial distribution of ion channels and transporters in cell migration. *Americal Journal of Physiological Society*, 2001.

[**58**] F. A. H. P. J. . S. C. Schwab, A. Role of ion channels and transporters in cell migration. *Physiology review*, 2012.

[**59**] C. O. G.-M. E. S. P. H. V. Sepúlveda N., Petitjean L. Collective cell motion in an epithelial sheet can be quantitatively described by a stochastic interacting particle model. *PLOS Computational Biology*, 9:3, 2013.

[**60**] F. V. C. . M.-B. Shin, K. Tight junctions and cell polarity. *Annual Review of Cell and Developmental Biology*, 2006.

[**61**] G. N. S.-P. M. G.-M. E. Shirley M., Shlomovitz R. and S. P. Physical model of the dynamic instability in an expanding cell culture. *Biophysical Journal*, 98:361:370, 2010.

[**62**] A. Z. Tamas Vicsek. Collective motion. *Physics Reports*, 2012.

[**63**] S. Thesleff. Nerve and muscle excitation, second edition. *Muscle & Nerve*, 4(6):533–533, 1981. ISSN 1097-4598. doi: 10.1002/mus.880040616. URL http://dx.doi.org/10.1002/mus.880040616.

[**64**] X. T.-M. M. J. J. F. a. D. A. W. Thomas E. Angelini, Edouard Hannezo. Glass-like dynamics of collective cell migration. *PNAS*, 12:4714:4719, 2011.

[**65**] A. Tremel, A. Cai, N. Tirtaatmadja, B. Hughes, G. Stevens, K. Landman, and A. OâĂŹConnor. Cell migration and proliferation during monolayer formation and wound healing. *Chemical Engineering Science*, 64(2):247 – 253, 2009. ISSN 0009-2509. doi: http://dx.doi.org/10.1016/j.ces.2008.10.008. URL http://www.sciencedirect.com/science/article/pii/S0009250908005356.

[**66**] A. T. M. E. W. D. B. J. Trepat .X, Wasserman M.R. and F. J.J. Physical forces during collective cell migration. *Nature Physics*, 5:426:430, 2009.

[**67**] A. T. M. E. W. D. B. J. P. Trepat X., Wasserman M. R. and F. J.J. Mechanical waves during tissue expansion. *Nature Physics*, 2009.

[**68**] L. C. Vedula E.R.K., Ravasio A. and L. B. Collective migration: a mechanistic perspective. *Physiology*, 28:370:379, 2013.

[**69**] J. E. Vermolen F.J. Computer simulations from a finite-element model for wound contraction and closure. *Journal of Tissue Viability.*, 19:43:53, 2010.

[**70**] M. T. L. G. C. G. Victor W. Wong, Satoshi Akaishi. Pushing back: Wound mechanotransduction in repair and regeneration. *Journal of Investigative Dermatology*, 131:2186–2196, 2011.

[**71**] P. Vitorino and T. Meyer. Modular control of endothelial sheet migration. *Genes Dev.*, 22:3268–3281, 2008.

[**72**] T. W. and S. E.J. Pivlab- time-resolved digital particle image velocimetry tool for matlab. 2014.

[**73**] K. C. R. Wegener, J. and I. Giaever. Electric cellâĂŞsubstrate impedance sensing (ecis) as a noninvasive means to monitor the kinetics of cell spreading to artificial surfaces. *Experimental Cell Research*, 2000.

[**74**] R. V. E. A. D. T. T. E. B. J. P. B. J. J. F. Xavier Serra-Picamal, Vito Conte and X. Trepat. Mechanical waves during tissue expansion. *Nature Physics*, 8:628–634, 2012.

[**75**] X. L. J. Q. C. T. Yu Wang, Guixue Wang. Substrate stiffness regulates the proliferation, migration, and differentiation of epidermal cells. *Burns*, 38:414:420, 2012.